

UC Irvine

UC Irvine Electronic Theses and Dissertations

Title

Community-Based Multi-Sensory Structural Health Monitoring

Permalink

<https://escholarship.org/uc/item/1nv4f49j>

Author

Alzughaibi, Ahmed

Publication Date

2022

Peer reviewed|Thesis/dissertation

UNIVERSITY OF CALIFORNIA,
IRVINE

Community-Based Multi-Sensory Structural Health Monitoring

DISSERTATION

submitted in partial satisfaction of the requirements
for the degree of

DOCTOR OF PHILOSOPHY

in Electrical and Computer Engineering

by

Ahmed Ali M Alzughhaibi

Dissertation Committee:
Professor Fadi Kurdahi, Chair
Professor Ahmed Eltawil
Professor Michael Green

2022

DEDICATION

This thesis is wholeheartedly dedicated to my beloved wife and daughters Seba, Dana and Lana; who have been my source of inspiration and gave me strength when I thought of giving up, who continually provide their emotional support.

To my father who have been supportive in every stage in my live.

To my wonderful deeply missed Mather and Grandmother. Forever you remain in my soul.

And lastly, to my brothers, sisters, friends who shared their words of advice and encouragement to finish this dissertation.

TABLE OF CONTENTS

	Page
LIST OF FIGURES	v
LIST OF TABLES	vii
LIST OF ALGORITHMS	viii
ACKNOWLEDGMENTS	ix
VITA	x
ABSTRACT OF THE DISSERTATION	xii
1 Introduction	1
1.1 Introduction and Background	1
1.2 Structural Damage Indicator	6
1.3 Hidden Structural Damage	7
1.4 Dissertation Organization	9
2 Initial Accelerometer-Based SHM System (Version 1.0)	10
2.1 Client Mobile-phone Application	11
2.2 Cloud Server	15
2.2.1 Database	16
2.2.2 Web page	17
2.3 Classification Process	20
2.4 Initial Accelerometer-based System Overview	24
2.5 Initial system Experimental Validation	25
2.6 Conclusion	28
3 Vision-based Monitoring	30
3.1 The use of Vision-based Techniques in SHM	31
3.2 The Development of Vision-based SHM Method	32
3.2.1 Feature Extraction	32
3.2.2 Feature Tracking	33
3.2.3 Scaling Factor (SF)	33
3.3 Vision-based Tracking Experimental Setup and Results	34
3.4 Conclusion	38

4	Multi-sensory System (Version 2.0)	39
4.1	Structural Health Classification Process	40
4.1.1	Vision Algorithm	40
4.1.2	Smartphone Sliding Detection	41
4.1.3	Camera Self-Calibration	42
4.1.4	Signal Preconditioning	44
4.1.5	Sensor Fusion Flow	45
4.2	Community-Based SHM Network	46
4.2.1	Smartphone Application	46
4.2.2	Cloud Server	48
4.2.3	Database	48
4.2.4	Visualization	50
4.3	Shake Table Validation	51
4.4	System Performance	55
4.5	Conclusions	60
	Bibliography	64
	A Inter-Story Drift Distribution	70

LIST OF FIGURES

	Page
1.1 Typical story drifts under earthquake excitation.	7
1.2 Holiday Inn Van Nuys, California seen from distance after 1994 Northridge earthquake.	8
1.3 Holiday Inn Van Nuys, California after 1994 Northridge earthquake.	9
2.1 Screenshots of the Client Application. The seismic sensing is performed silently in the background. The information is fed back to the user in the form of a disaster map.	11
2.2 Mobile-phone Application Flowchart. The left hand side shows different application modes.	12
2.3 The EC2 Cloud Server Flowchart	15
2.4 Website Screenshot. A detailed map is shown containing buildings tagged with their most likely structural health status.	17
2.5 Satellite view showing the terrain surrounding the targeted buildings.	18
2.6 Street-view feature makes searching for buildings even easier for the public	18
2.7 Screenshots of the Client Application Disaster Map. The information is fed back to the user in the form of a disaster map.	19
2.8 The EC2 Cloud Server Flowchart. The chart shows signal processing of received phone acceleration signals.	24
2.9 System Flowchart. The left hand side shows the mobile-phone application modes. The right hand side describes the signal processing of received phone acceleration signals.	26
2.10 Error in IDR Using Smart-phone Accelerometer. Different settings and features were tested.	28
3.1 Image of a typical office ceiling. Red crosses in the image are the detected features from the accelerated segment test (FAST) algorithm.	33
3.2 Vision-based Structural Health Monitoring algorithm Process	34
3.3 Shake table setup used in the experiment	35
3.4 Displacement extracted using proposed camera based SHM approach in red, and reference in blue	36
3.5 Error in displacement extracted using proposed camera based SHM approach	37
3.6 One cycle of displacement extracted using our camera based SHM approach in red, and from the reference in blue	37

4.1	Overview of the structural health classification process used in the proposed multi-sensory structural health monitoring (SHM) system. The red labels on the arrows represent the quantity being measured and its units. The dashed-green block in the upper right highlights the vision algorithm, which obtains the camera records of the ceiling movement and outputs pixel inter-story drift data. The dashed-blue block in the middle (on the left) highlights the self-calibration algorithm preceded by signal preconditioning; this block obtains the inter-story acceleration and pixel inter-story drift and outputs the scaling factor k	47
4.2	The smartphone application process. Seismic sensing is performed silently in the background.	49
4.3	Screenshots of the smartphone application. The seismic sensing is performed silently in the background. The building's structural safety status is fed back to the user in the form of a disaster map.	50
4.4	Website screenshot. A detailed map is shown containing buildings tagged with their most likely structural health status.	51
4.5	The proposed community-based SHM network layout. The smartphone app process is explained in Section 4.2.1 and Figure 4.2. The server process is discussed in Section 4.1 and Figure 4.1. The disaster map is visualized in Figure 4.3 and Figure 4.4.	52
4.6	Shake table experimental setup. The reference accelerometer (Model393C [1]) was attached to the shake table, which is shown on the right hand side.	54
4.7	The procedures followed in each experiment.	55
4.8	True inter-story drifts (dashed black lines) plotted with the drift estimated using the proposed algorithm (solid red lines). The drifts estimated using the proposed algorithm show good agreement with the ground truth. The smartphone model and excitation signal for each experiment were: (a) SMG900T with a sinusoidal excitation of 34.7 mm peak-to-peak amplitude and 4 Hz frequency, (b) SMG920V#1 with a sinusoidal excitation of 25.6 mm peak-to-peak amplitude and 5 Hz frequency, (c) SMG920V#2 with a sinusoidal excitation of 18.2 mm peak-to-peak amplitude and 6 Hz frequency, and (d) SMG920V#2 with a sinusoidal excitation of 13.0 mm peak-to-peak amplitude and 7 Hz frequency.	56
4.9	The performance of the proposed SHM system, plotted as the p_e for different distributions of inter-story drifts with a specific μ_s and σ_s (i.e., for different building types and under earthquake excitations of different intensities). The expected p_e values when an 8-story building is hit by an earthquake with hazard levels corresponding to a 2% probability of exceedance in 50 years, 10% in 50 years, and 50% in 50 years are highlighted in the plot. The performance of the system that uses seismic-grade accelerometers (KB12VD) is plotted for comparison.	59

LIST OF TABLES

	Page
1.1 Main earthquake monitoring methods currently in use	5
1.2 Classification thresholds of steel moment-frame buildings using peak IDR [2].	6
3.1 Sinusoidal shaking of different amplitudes and frequencies	36
4.1 The tested smartphones' technical specifications.	53
4.2 Experimental parameters and accuracy achieved by each phone represented by the standard deviation of the error (σ_e). Excitation in the form of sinusoidal shaking of different amplitudes and frequencies was applied to the shake table.	57
4.3 Probability of structural damage classification error p_e using the proposed SHM system for different earthquake hazard levels; p_e values for other SHM systems for the same earthquake hazard levels are listed for comparison. . . .	60

LIST OF ALGORITHMS

	Page
1 Mobile-phone Application	13
2 Removing the Bias	20
3 Displacement Calculation	22
4 IDR calculation	23
5 Structural health classification process	25

ACKNOWLEDGMENTS

I would like to express the deepest appreciation and gratitude to my advisor, Professor Ahmed Eltawil, for his exceptional guidance, motivation and support throughout this academic journey. Without his persistent help and thoughtful insight, this research would not have been possible.

I would like to thank Professor Fadi Kurdahi for his insightful comments and advice.

I would like to thank Professor Michael Green for being part of my dissertation committee and for the insights that helped improving this work.

Very special thanks to Dr. Ahmed Ibrahim, who is a good friend of mine and the co-author/researcher in the research project. His extensive understanding, experience and continuous help have paved the way to continue this research with the best background, knowledge and experiments setup.

Also special thanks to my lab mates and colleagues Mohammad Almajhadi, Ibrahim Alquaydheb, Mohamed Fouda, Ahmed Eisa and Michael Ayoub for all of the support and encouragement that helped immensely to complete this degree.

Moreover, a message of recognition to my sponsors Qassim University and the Saudi Arabian Cultural Mission.

VITA

Ahmed Ali M Alzughaibi

EDUCATION

**Doctor of Philosophy in Electrical
Engineering and Computer Science**
University of California, Irvine

2022
Irvine, California

**Master of Science in Electrical
Engineering and Computer Science**
University of California, Irvine

2018
Irvine, California

Bachelor of Science in Electrical Engineering
Qassim University

2011
Qassim, Saudi Arabia

RESEARCH EXPERIENCE

Graduate Research Assistant
University of California, Irvine

2015–2022
Irvine, California

TEACHING EXPERIENCE

Teaching Assistant
Qassim University

2011–2015
Qassim, Saudi Arabia

REFEREED JOURNAL PUBLICATIONS

Community-Based Multi-Sensory Structural Health Monitoring System: A Smartphone Accelerometer and Camera Fusion Approach **2021**
IEEE Sensors Journal

REFEREED CONFERENCE PUBLICATIONS

Post-Disaster Structural Health Monitoring System Using Personal Mobile-Phones **Jan 2019**
IEEE Topical Conference on Wireless Sensors and Sensor Networks (WiSNet)

Vision-based Structural Health Monitoring Utilizing Citizen-owned Smart-phones **May 2020**
IEEE International Instrumentation and Measurement Technology Conference (I2MTC)

ABSTRACT OF THE DISSERTATION

Community-Based Multi-Sensory Structural Health Monitoring

By

Ahmed Ali M Alzughhaibi

Doctor of Philosophy in Electrical and Computer Engineering

University of California, Irvine, 2022

Professor Fadi Kurdahi, Chair

Assessing the structural integrity of buildings after an earthquake is necessary for citizens to be able to use these facilities safely after the event. The currently available structural health monitoring (SHM) systems use a dense network of sensors installed in buildings to monitor their behavior during earthquakes. Such a network is impractical with respect to cost and deployment time for the vast majority of buildings; therefore, most structures remain uninstrumented. However, a massive network of citizen-owned smart devices, such as tablets and smartphones that contain cameras and vibration sensors, has already been deployed. This research develops a framework that can crowdsource readings from distributed citizen-owned smart devices and convert these readings into actionable information. Although prior community-based seismic research focused on using smartphones to provide early disaster warnings, the proposed system focuses specifically on using video captured on a smartphone to directly assess the structural health of buildings post-earthquake, thus providing citizens and emergency personnel with immediate relevant information regarding the health state of buildings. This research presents a novel self-calibration technique for a smartphone camera using its internal accelerometer readings. The system's performance is studied using shake-table experiments with different shaking scenarios. Shake table experiments show that the proposed technique can achieve sub-millimeter accuracy, demonstrating its suitability for SHM applications.

Chapter 1

Introduction

1.1 Introduction and Background

The prolific construction of multi-story buildings over the past century has enabled cities to grow and fulfill the demands of people and businesses. However, given the lack of large-scale structural health assessment methods, unsound infrastructure in earthquake-prone areas could threaten millions of lives when they are hit by an earthquake [3]. In the United States, 28 million people live in areas classified as being at high risk of earthquakes [4]. The United States Geological Survey (USGS) and the Structural Engineers Association of Northern California reported that about one-tenth of multi-story structures in San Francisco would likely collapse in response to a major earthquake similar to the one that struck the city in 1906 [5]. A reliable method for detecting hidden building damage is essential as many damaged buildings do not collapse at the time the earthquake strikes, but rather, days or weeks afterwards [6]. Structural health monitoring (SHM) systems, which are automated methods to continually track a structure's safety, have received significant attention lately because of the systems' potential impacts from both economic and safety standpoints [7, 8, 9].

There are multiple types of SHM systems. Vibration-based SHM systems use vibration-based sensors to detect damage in structures by tracking variations in modal parameters (i.e., natural frequencies and mode shapes) [10, 11]. In [12], a wireless network of accelerometer sensors connected via radio-frequency identification (RFID) tags was used to continuously record the acceleration of a structure. The records were then used to estimate the structure's damage state via variations in natural frequencies. The system was then extended by [13] by adding a strain gauge to the sensing chip as an additional measure of natural frequency variations because strain readings identify the local damage to the structure (e.g., cracks, corrosion) with a higher sensitivity. In [14], a wired network of accelerometers and piezoelectric transducers was constructed to track variations in mode shapes for structural fault localization. In [15] and [16], a network of accelerometers mounted to floors of a building was constructed to detect damage to nonstructural elements, such as gas pipes and built-in medical equipment.

Vibration-based methods are relatively low cost, which is the main reason for their adoption in most SHM systems [10]; however, they are vulnerable to ambient conditions, i.e., variations in the modal parameters could occur for reasons other than structural damage, such as changes in humidity and temperature [17]. In contrast, studies showed that displacement-based SHM, specifically the inter-story drift ratio (IDR), which is the relative translational displacement between two consecutive floors [17], correlates best to both global and local structural damage due to earthquakes [18, 19, 17].

Several displacement-based SHM systems have been presented in the literature and use various direct displacement measurement sensors, such as cameras, lasers, and radar. In [20], a frequency-modulated continuous-wave (FMCW) radar-based SHM system was installed in a building to measure the IDR. The system works by transmitting a signal to a reflector placed in the opposite corner of the building and measuring changes in the returned echo's time of travel, which is related to the inter-story displacement. Additionally, an SHM system

that uses a camera as the displacement measuring tool was created [21]. The system uses action cameras to capture the movement of a bridge in response to crossing trucks to assess its structural integrity, considering the weight of the truck. In another system, a smartphone camera, mounted on a reference steel frame, was used to infer the displacement of a suspension bridge model in a laboratory by tracking a pre-installed target with predefined dimensions [22].

Relatively recently, several buildings' SHM systems started using cameras to track the horizontal movement of floors during earthquake shaking. Feng et. al. [23], created a SHM setup using a camera, optical lens and a Laptop computer. The camera is set up on a stand outside of a building (off-structure) to estimate the floors horizontal movements by track multiple artificial or natural (e.g. bolts) targets. Park et. al. [24], used a setup containing 3 cameras placed in different predetermined locations outside of a building (off-structure) to monitored its 3-dimensional movement. Zhang et. al. [25] proposed tracking the inter-story drifts by installing cameras on the outside walls of a building (on-structure) and markers on each floor level; removing the need for an off-structure reference point.

However, the displacement-based systems that are currently in use require either manual harvesting of sensor records or a wired/wireless local network to connect the sensors. Because of the cost and time required, achieving widespread deployment of such networks is infeasible. As a result, most currently standing structures remain unmonitored [26]; therefore, the only post-earthquake assessment method currently used for these structures is physical on-site inspection by teams of engineers. Manual assessment can take months to be completed after a major seismic event, which could potentially lead to structural failure when internal structural damage is present despite the lack of visible external signs.

To tackle the scalability issue, this paper proposes the use of community-owned smart devices to monitor the structural health of buildings during earthquakes. Several studies have proposed the use of community-based sensor-integrated devices for seismic applica-

tions, a system that would benefit from the widespread availability of smart devices that are connected to the Internet. An early earthquake warning (EEW) system, referred to as MyShake, was developed using citizen-owned smartphone accelerometer data [27, 28, 29]. MyShake successfully detected and provided a 20-second warning for a magnitude 5 (M5) earthquake. Additionally, an earthquake monitoring system, Community Seismic Network (CSN), creates dense ground-shaking map using community-hosted mini-seismometers and smartphones [30, 31, 32].

Going well beyond the efforts of MyShake and CSN, which use smartphones to communicate early warnings and create shaking maps, respectively, this paper proposes using smartphones to detect earthquake events and smartphone cameras to track a structure’s movement. The records are then uploaded to a cloud server for post-earthquake processing in order to help infer the structure’s health state. Damaged structures are reported to first responder officials and visualized on a publicly available website in the form of a disaster map where structures are marked with their most likely damage state.

In this research, an SHM system that can handle inputs from multiple smartphones across different floors of a building and across multiple buildings was constructed. The proposed system is fully scalable to cover additional cities, states, and countries due to the use of a cloud-based server that can process thousands of readings. The system’s performance is studied using several shake-table experiments of different shaking scenarios. The proposed SHM system achieves sub-millimeter accuracy, which far exceeds the SHM accuracy requirements previously reported [33, 34]. The performance of the proposed SHM system, quantified by the probability of classification errors is discussed and compared with other recently developed SHM systems. For the purposes of this work, it was assumed that citizens would be motivated to install the required application on their devices, as they will benefit directly from the early warning. Table 1.1 summarizes main earthquake monitoring methods

currently in use.

Table 1.1: Main earthquake monitoring methods currently in use

SHM methods	Speed	Accuracy	Initial cost	Operational cost	Scalability
Physical Inspection	slow	moderate	N/A	very high	very low
Traditional SHM systems (dedicated sensors and network)	fast	high	very high	high	low
Community seismic network (dedicated sensors but community-based network)	fast	moderate	moderate	moderate	moderate
Smartphone-accelerometer-based SHM	fast	low	low	low	high

The main contributions of this work can be summarized as follows:

1. Proposing an SHM mechanism that estimates a building's IDR using smartphones within the structure;
2. Proposing a novel self-calibration technique for a smartphone camera using the smartphone's internal accelerometer readings;
3. Developing a community-based SHM network that consists of a smartphone application, a cloud-based server, and a website-integrated disaster map;
4. Validating the reliability and accuracy of the proposed multi-sensory algorithm using a seismic shake table;

5. Estimating the probability of structural health misclassification using the proposed SHM system.

1.2 Structural Damage Indicator

According to the Federal Emergency Management Agency (FEMA), the relative horizontal displacement between adjacent floors is related to building health [2] via the IDR, which can be used to classify structures into three categories—immediate occupancy (IO), collapse prevention (CP), or collapse likely (CL)—depending on the peak value of the IDR. The IDR of two consecutive floors of a multi-story building is the inter-story drift divided by the floor height, as shown in Fig. 1.1. IDR is calculated using Equation (1.1). The peak IDR value is then compared to the classification limits, as shown in Table 1.2. This process is repeated for all adjacent floors in a given building.

Table 1.2: Classification thresholds of steel moment-frame buildings using peak IDR [2].

Peak IDR %	Building State
IDR < 0.7%	Immediate occupancy (IO)
0.7% < IDR < 5%	Collapse prevention (CP)
IDR > 5%	Collapse likely (CL)

$$IDR = \left| \frac{displacement_{upper\ floor} - displacement_{lower\ floor}}{Floor\ Height} \right| \quad (1.1)$$

For example, for a steel moment frame building with a 4 m floor height, a drift of over 200 mm (IDR > 5%, also written as 0.05 IDR) between any adjacent floors in the building makes it unsafe; therefore, it is classified as CL. If the drift is between 28 and 200 mm (0.7% < IDR

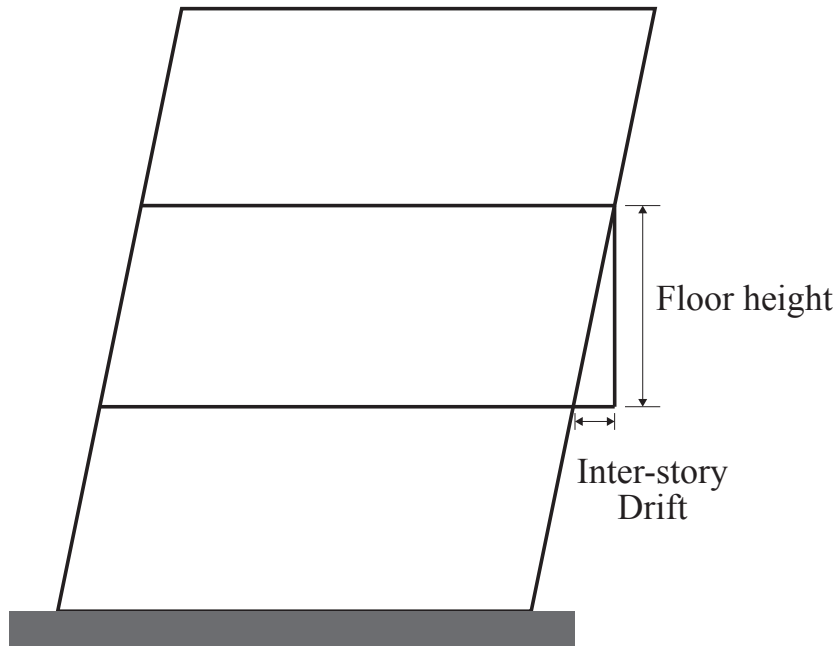


Figure 1.1: Typical story drifts under earthquake excitation.

$< 5\%$), the building is classified as CP (requiring further assessment); a building with drifts less than 28 mm (IDR 0.7%) is considered IO (safe). The building type and the floor heights are available from the city tax assessor's office, popular GPS tools, or reported by building owners or managers. For buildings with no currently reported building type or floor heights, the IDRs could be based upon the best available estimates until those are refined as more data becomes available.

1.3 Hidden Structural Damage

When a major earthquake hit a city, few buildings would partially or completely collapse. However, many more buildings would not show any visible damage, despite suffering from a severe structural damage; which make them vulnerable to collapse during the earthquake

aftershocks or future events. For example, a hotel in Van Nuys, California has been damaged during the Northridge earthquake in 1994. Although there is no noticeable damage when seen from a distance (Figure 1.2), the main columns of the building have been severely damaged (Figure 1.3).



Figure 1.2: Holiday Inn Van Nuys, California seen from distance after 1994 Northridge earthquake.



(a) Exterior up-close view of the column damage caused by the earthquake



(b) Interior up-close view of the column damage caused by the earthquake

Figure 1.3: Holiday Inn Van Nuys, California after 1994 Northridge earthquake.

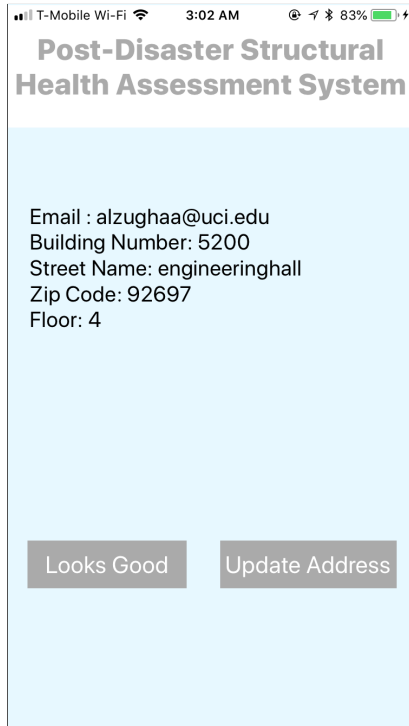
1.4 Dissertation Organization

The rest of the dissertation is organized as follows. Chapter 2 introduces the initial accelerometer-based SHM system. Chapter 3 reviews the proposed vision-based structural health monitoring methodology. Finally, chapter 4 presents the proposed community-based multi-sensory SHM system.

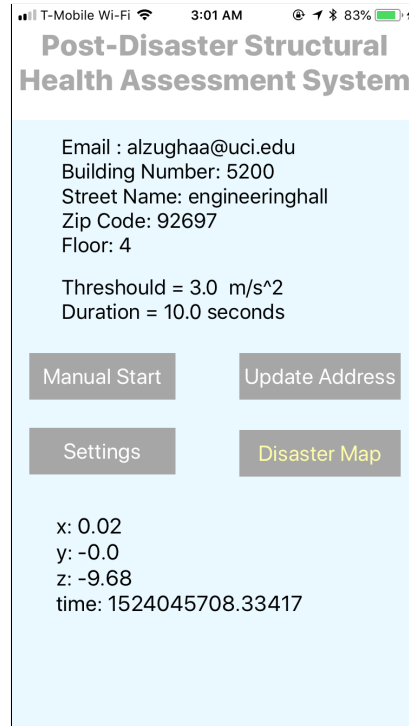
Chapter 2

Initial Accelerometer-Based SHM System (Version 1.0)

This section reviews the development initial accelerometer-based SHM system. The system was designed using client-server architecture. The user application is used to detect, store and then send recorded sensor data to a centralized cloud server. Then, the server sorts, organizes and stores data in a database. When requested by the user, the server computes the IDR value for each building and classifies the building to IO, LS or CP. Then, the server generates a map that displays buildings tagged with their structural health status. The rest of the chapter is organized as follows. Section 2.1 gives an overview of the mobile-phone application. Section 2.2 covers the server's architecture. the classification process is presented in section 2.3. Finally, the experiments conducted for the initial system are reported in section 2.5.



(a) Welcome page



(b) Main UI

Figure 2.1: Screenshots of the Client Application. The seismic sensing is performed silently in the background. The information is fed back to the user in the form of a disaster map.

2.1 Client Mobile-phone Application

As part of this work, we developed a mobile-phone application that detects an earthquake and sends sensor readings to a centralized cloud computing server along with the exact time, device ID, user email address, building's street address, and floor number. Screen-shot of the iOS application are in Figure 4.3.

The app consists of 3 modes: steady mode, trigger mode, and streaming mode. The app has to enter a steady state before it can be active and available to get excited by an earthquake to avoid any additional noise in the reading. The app enters the steady mode when the absolute sensed acceleration in the x-y direction is below a certain threshold for certain time window. Trigger stage starts once an earthquake is detected, i.e. predetermined threshold

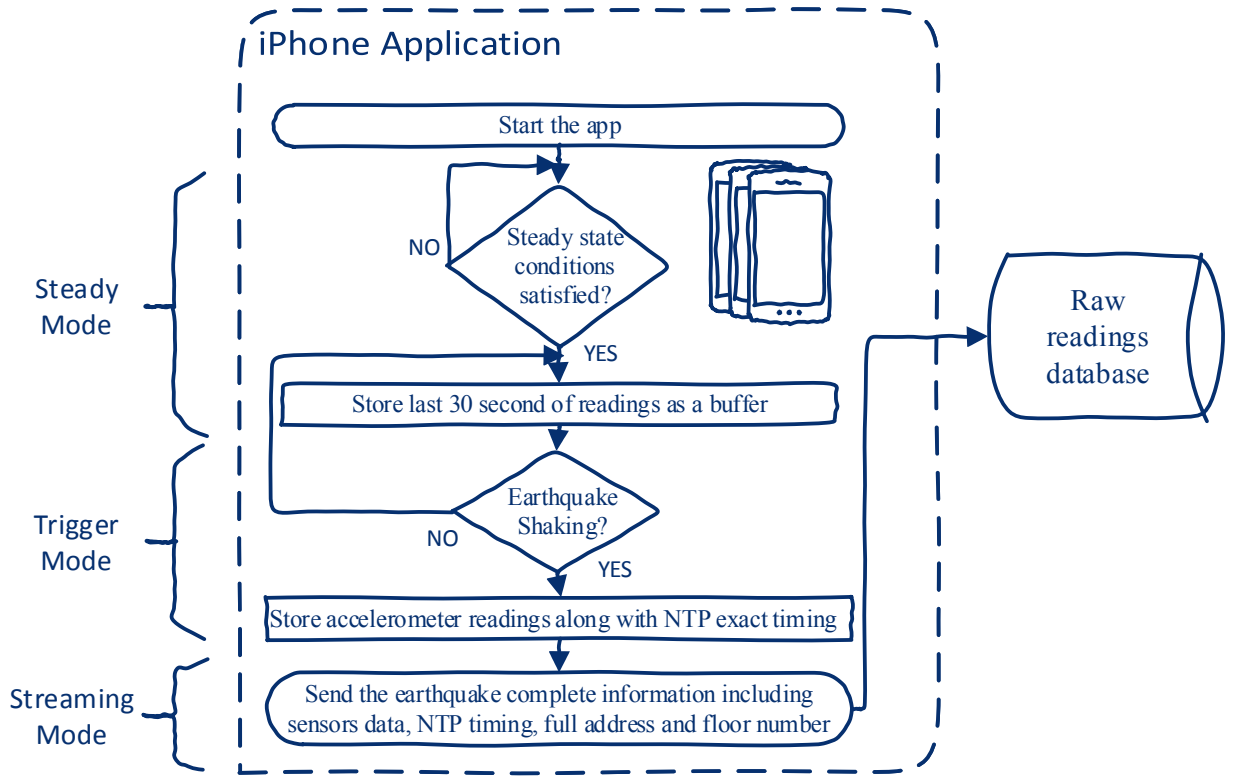


Figure 2.2: Mobile-phone Application Flowchart. The left hand side shows different application modes.

(0.1g) has been crossed in the x-y direction. This is the same technique that has been used in iShake [27]. The app stores readings for a specific duration. After that, the app begins sending the recorded event information and readings to the centralized cloud-server. An overview of how the app works is shown in Figure 2.2. The detailed detection mechanism and signal processing of the mobile-phone application is presented in Algorithm 1.

Sampling Rate

According to Apple developers documentation, The maximum frequency at which you can request updates is hardware-dependent [35]. In our experiments, the highest sampling fre-

Algorithm 1 Mobile-phone Application

1: **INPUT** *shaking, and location information*
2: **OUTPUT** *acceleration as a function of time*
3: **for** $i \leftarrow 1, 2, \dots, f_s * T_{steady}$ **do** $\triangleright f_s$ is the sampling rate, and T_{steady} is the pre-defined duration of the steady state condition
4: $a_{x_i}, a_{y_i},$ and $a_{z_i} \leftarrow$ accelerometer reading in the x-axis, y-axis, and z-axis, *respectively*
5: $a_{xy_i} \leftarrow \sqrt{a_{x_i}^2 + a_{y_i}^2}$
6: **end for**
7: **while** $\max\{a_{xy}\} < \Theta_{steady}$ **AND** $a_{z_i} > 9.0$ **do** $\triangleright \Theta_{steady}$ is the pre-defined threshold of the steady state condition
8: **if** $a_{xy} > \Theta_{detection}$ **then** $\triangleright \Theta_{detection}$ is the pre-defined earthquake detection threshold
9: **for** $i \leftarrow 1, 2, \dots, f_s * T_{storing}$ **do** $\triangleright T_{steady}$ is the pre-defined duration of the earthquake readings
10: $a_{x_i}, a_{y_i},$ and $a_{z_i} \leftarrow$ accelerometer reading in the x-axis, y-axis, and z-axis, *respectively*
11: $a_{t_i} \leftarrow$ current NTP epoch time
12: **end for**
13: **else**
14: Check steady state conditions again
15: **end if**
16: **end while**
17: *Raw readings database* $\leftarrow a_x, a_y, a_z, a_t,$ and location information

quency for both devices is 100 Hz, so this was used in the experiment. This frequency is twice as much as what was used in MyShake [28].

Pre-Trigger

If the data is recorded at the start of the trigger time, the prior data will be lost. It is worth noting that an error at the beginning of the acceleration time window is amplified by double integration, which is needed to calculate the displacement (see section 2.3 for the details). For that reason, a moving buffer was added to store accelerometer data for 30 seconds. The stored data is then sent to the server when the app is triggered.

NTP-Time Synchronization

Calculating relative displacements (*IDR*) requires millisecond accuracy for precision phasing. Therefore, a synchronization technique is required across phones to avoid clock drift. The proposed application uses *Network Time Protocol* (NTP) timing to ensure an accurate simultaneous reference for all devices [36], [37]. NTP is the Internet protocol used to synchronize the clocks of computers to some time reference. The time reference used in the proposed system is epoch time which is the total number of seconds since midnight of January 1, 1970. The error in calculating the displacement using the mobile-phone internal clock for Synchronization compared with using NTP clock is discussed in the section 2.5.

Running in the Background

One key feature of the application is the ability to detect earthquakes while running in the background. In other words, even if the user is not directly interacting with the application interface the app is still sensing the acceleration and can switch between the internal modes.

2.2 Cloud Server

Using a cloud server has major advantages over using a standard server. One advantage is the scalability of the cloud server which is crucial property in seismic related systems because it is hyperactive for a short period of time during and after an event [38]. Low operational cost is another attractive feature of cloud servers compared to standard servers. In addition, in cloud services maintenance and back up are usually offered by the service provider. *Amazon Web Services* (AWS) is one of the major cloud computing service providers which make it suitable for the proposed system. An Amazon *Elastic Compute Cloud* (EC2) is used as a base for all computations and processes needed. An overview of how the EC2 server is presented in Figure 2.3.

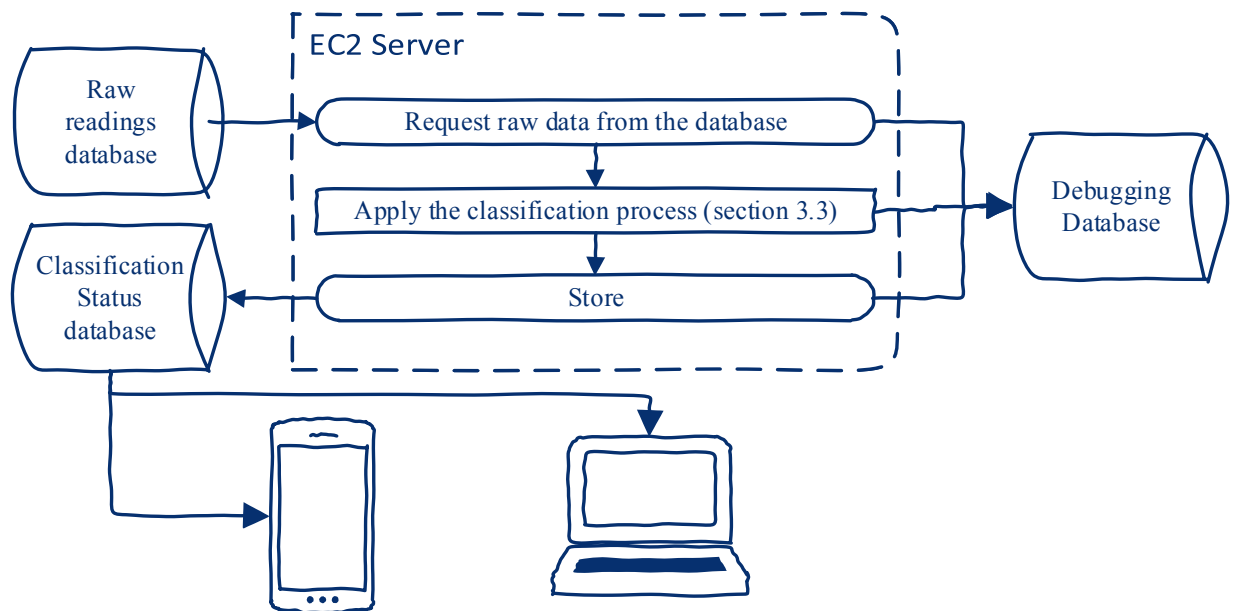


Figure 2.3: The EC2 Cloud Server Flowchart

2.2.1 Database

The system uses a cloud-based MySQL database because of its ability to store and organize thousands of readings to be called back when needed. The data is organized by zip code, street address, and floor number. The system consists of 3 different databases. One database is used to store raw sensor data received from the app along with the location information. Another database used to store the resultant IDRs for each building along with the exact time and date of the incident (earthquake). The last database is used as checkpoints for system debugging.

Raw Readings Database

The raw readings database is used to store raw sensor data received from the app along with the NTP timing of the readings. Location, date, and time of the incident are registered as well.

Classification Status Database

The classification status database is used to store the resultant IDRs for each building along with the exact time and date of the incident (earthquake).

Debugging Database

The debugging database provides checkpoints. Debugging database A is used to compare the received data to the data that was sent by the app. Debugging database B is used to ensure that the displacement calculation was done correctly. Finally, debugging database C is used to check the synchronization and relative displacement processes.

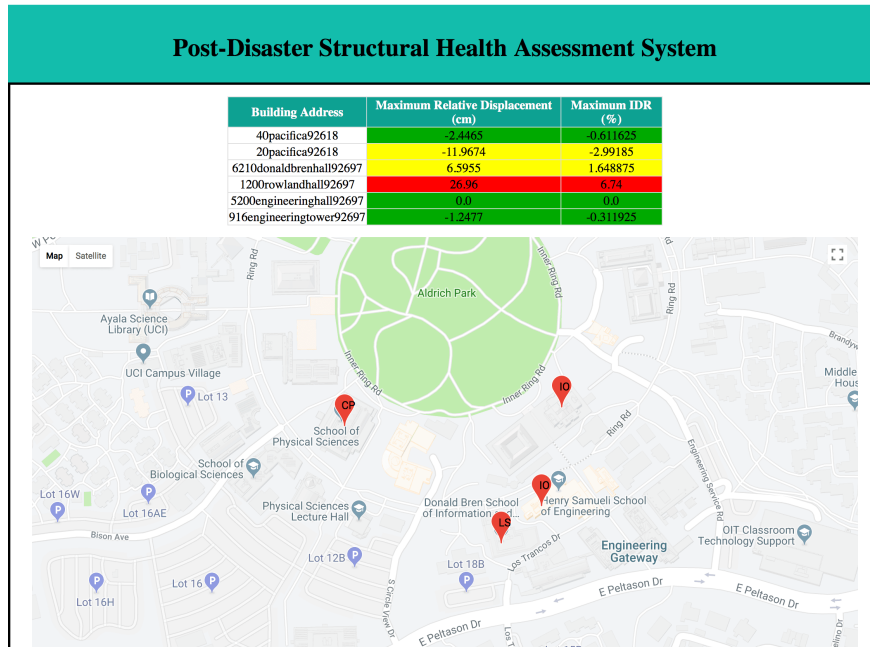


Figure 2.4: Website Screenshot. A detailed map is shown containing buildings tagged with their most likely structural health status.

2.2.2 Web page

A list of the tested buildings along with their classification status is displayed on the system's website which is also hosted by the EC2 server. In addition, the website includes a map of the buildings tagged with their structural health state making it easier for the public to check their buildings in the aftermath of an event. A screen-shot of the web page is shown in Figure 4.4. Furthermore, the list and the map are available in the app. A satellite view showing the terrain of the building surroundings is also provided in the webpage, as in Figure 2.5. The street-view is another option provided in the website to make it easier for the public to search for their building's structural health status. Figures 2.6, 2.7 present the street-view feature in the website and the smart-phone's application, respectively.



Figure 2.5: Satellite view showing the terrain surrounding the targeted buildings.

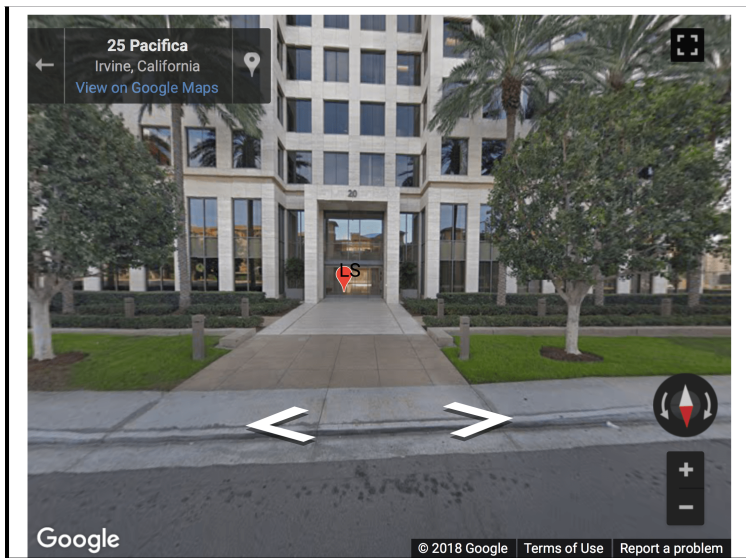
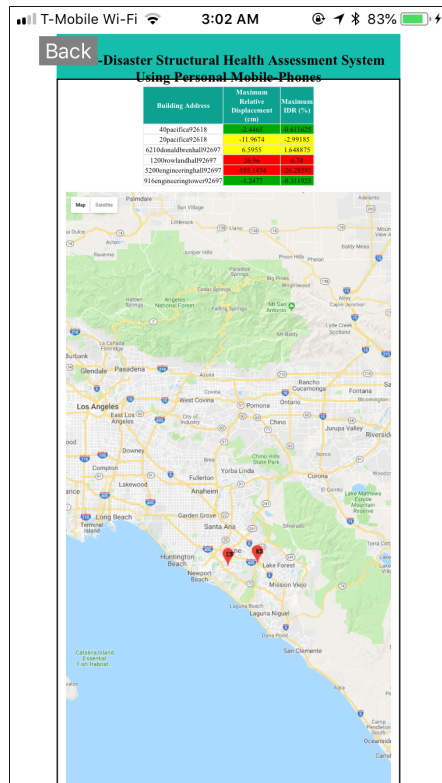
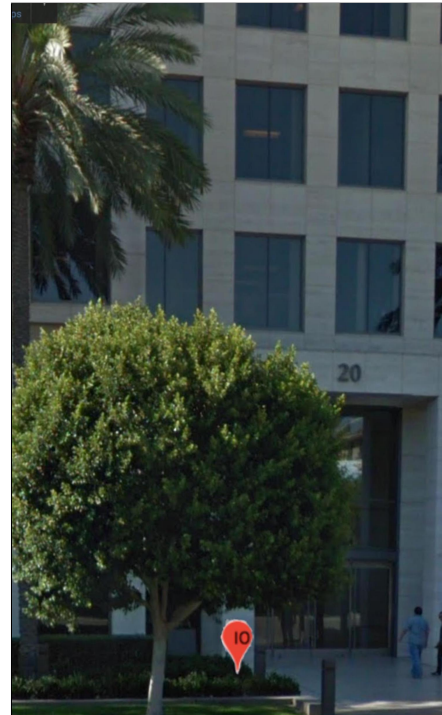


Figure 2.6: Street-view feature makes searching for buildings even easier for the public



(a) a list of the tested buildings search-able by street address or zip code in addition to the detailed map containing buildings tagged with their structural health status



(b) the street view feature allows the user to use phone's orientation to clearly point to the building

Figure 2.7: Screenshots of the Client Application Disaster Map. The information is fed back to the user in the form of a disaster map.

2.3 Classification Process

The system loops over all the buildings that have active users during the disaster to categorize them into IO, LS or CP using FEMA standard [39]. Classifying a building is done through several stages. These stages are:

Removing the Bias

Phone accelerometers usually have a constant bias. The first step is removing the bias for each axis of the acceleration which is estimated by long-term averaging. First the long-term mean (bias) needs to be calculated for each axis. After that, the long-term mean (bias) has to be subtracted from each reading in every axis. The pseudo-code for removing the bias process is given in Algorithm 2.

Algorithm 2 Removing the Bias

```
1: INPUT  $a_{x_{row}}[n], a_{y_{row}}[n]$ 
2: OUTPUT  $a_x[n], a_y[n]$ 
3:  $\mu_x \leftarrow \text{mean}(a_{x_{row}}[n])$ 
4:  $\mu_y \leftarrow \text{mean}(a_{y_{row}}[n])$ 
5: for  $i \leftarrow 1, 2, \dots, N$  do
6:    $a_x[i] \leftarrow a_{x_{row}}[i] - \mu_x$   $\triangleright$  removing the long-term average from every reading in x-axis
7:    $a_y[i] \leftarrow a_{y_{row}}[i] - \mu_y$   $\triangleright$  removing the long-term average from every reading in y-axis
8: end for
```

Displacement Calculation

Finding velocity as a function of time $v(t)$ from raw accelerometer data $a(t)$ is done using equation 2.1

$$v(t) = v_0 + \int_0^t a(t) dt \tag{2.1}$$

The initial velocity (v_0) = 0 because of the steady mode conditions. Furthermore, displacement $d(t)$ is found using equation 2.2

$$d(t) = d_0 + \int_0^t v(t) dt \quad (2.2)$$

The initial displacement (d_0) = 0 because of the steady mode conditions. In short, integrating the acceleration results in velocity while double integrating the acceleration calculates displacement as in equation 2.3.

$$d(t) = \int_0^t \left(\int_0^t a(t) dt \right) dt \quad (2.3)$$

Integration is done numerically by summation in the case of digital (discrete) signals. Equations 2.1, 2.2, and 2.3 can be rewritten as follows

$$v[n] = dt \sum_0^n a[n] \quad (2.4)$$

$$d[n] = dt \sum_0^n v[n] \quad (2.5)$$

$$d[n] = (dt)^2 \sum_0^n \sum_0^n a[n] \quad (2.6)$$

where dt is the inverse of the sampling rate (f_s) ; $dt = 1/f_s$. $d[n]$ is the displacement at time n . The function *cumsum* (cumulative summation) is used to approximate integration.

cumsum is defined in 2.7.

$$cumsum(g[n])[i] = \sum_{k=1}^i g[k] \quad \text{for } i = 1, 2, \dots, N \quad (2.7)$$

Where $g[n]$ is a discrete sequence. For example, the cumulative sums of the sequence $\{a, b, c, d, e, \dots\}$, are $\{a, a + b, a + b + c, a + b + c + d, a + b + c + d + e, \dots\}$. Furthermore, the double cumulative sums (double integration) of the sequence $\{a, b, c, d, e, \dots\}$, are $\{a, 2a + b, 3a + 2b + c, 4a + 3b + 2c + d, 5a + 4b + 3c + 2d + e, \dots\}$. Note that the effect of the noise in the beginning of a signal distorts the resultant signal much more severely than the noise at the middle or end of it. The pseudo-code for displacement calculation procedures is given in Algorithm 3.

Algorithm 3 Displacement Calculation

```

1: INPUT  $f_s, t[n], a[n]$ 
2: OUTPUT  $d[n]$ 
3:  $f_s \leftarrow round(\frac{t[N]-t[1]}{N})$ 
4:  $dt \leftarrow 1/f_s$ 
5: for  $i \leftarrow 1, 2, \dots, N$  do
6:    $cumsum(a[n])[i] = \sum_{k=1}^i a[k]$ 
7:    $cumsum(v[n])[i] = \sum_{k=1}^i v[k]$ 
8: end for
9:  $v[n] \leftarrow dt * cumsum(a[n])$   $\triangleright v_0 = 0$  because of the steady mode conditions
10:  $d[n] \leftarrow dt * cumsum(v[n])$   $\triangleright d_0 = 0$  because of the steady mode conditions

```

Data Synchronization

Data must be aligned before relative displacement calculation. NTP time that was sent from the app, as mentioned in section 2.1, is used as the base of alignment.

Relative Displacement Computation

The server loops over every adjacent floor in every building containing active devices during an earthquake. Then, the IDR is computed using equation (2.8).

$$IDR_i = \max \left\{ \left| \frac{d[n]_i - d[n]_{i+1}}{h} \right| \right\} \quad (2.8)$$

Where IDR_i is the maximum IDR value between floor i and floor $i + 1$. $d[n]_i$ and $d[n]_{i+1}$ are the calculated displacements in meters for floor i and floor $i + 1$, respectively. h is the floor height in meters. After that, an equivalent IDR value is calculated for every building using equation (2.9).

$$IDR_b = \max \{ IDR_i : i = 1, 2, \dots, M - 1 \} \quad (2.9)$$

Where IDR_b is the maximum IDR value recorded between any adjacent floors in building b and M is number of floors in building b . Finally, a class is given to the building by comparing IDR_b with the FEMA reference values. The pseudo-code for relative displacement and IDR_b calculation procedures is given in Algorithm 4.

Algorithm 4 IDR calculation

- 1: **INPUT** $h, d[n]_S$
 - 2: **OUTPUT** IDR_b
 - 3: **for** $i \leftarrow 1, 2, \dots, M - 1$ **do**
 - 4: **for** $j \leftarrow 1, 2, \dots, N$ **do**
 - 5: $d[j]_{i_{relative}} \leftarrow \frac{d[j]_{S_i} - d[j]_{S_{i+1}}}{h}$ \triangleright where $d[j]_{i_{relative}}$ is the relative displacement between floors i and $i + 1$
 - 6: **end for**
 - 7: $IDR_i \leftarrow \max \{ |d[n]_{i_{relative}}| \}$
 - 8: **end for**
 - 9: $IDR_b \leftarrow \max \{ IDR_m \}$ $\triangleright m = 1, 2, \dots, M-1$
-

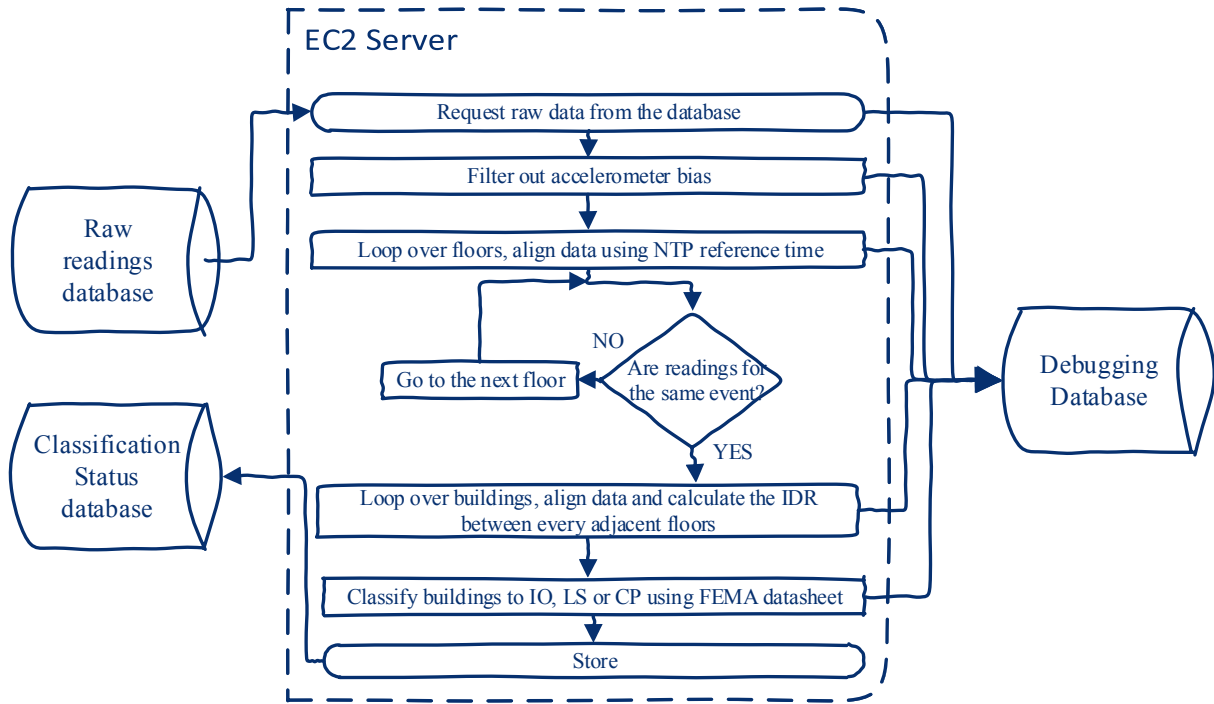


Figure 2.8: The EC2 Cloud Server Flowchart. The chart shows signal processing of received phone acceleration signals.

An overview of how the server classification process is given in Figure 2.8. The pseudo-code for the classification process is given in Algorithm 5.

2.4 Initial Accelerometer-based System Overview

A post-earthquake automated assessment system was built using client-server architecture. For the client side, an iPhone application was designed for earthquake detection. Once the earthquake is detected, the application saves the accelerations of the shaking. When the recording is finished, they are sent to the raw readings database which is used to register the unprocessed sensors readings, NTP timing and location details.

Algorithm 5 Structural health classification process

```
1: INPUT accelerometer readings, and building heights
2: OUTPUT structural health status
3: for Building in the targeted area do
4:   for floors in the building do
5:      $a_i[n] \leftarrow a_{i_{row}}[n]$   $\triangleright$  Filtering out the bias using Algorithm 2
6:      $d_i[n] \leftarrow a_i[n]$   $\triangleright$  the displacement is calculated for every floor using Algorithm 3
7:      $d[n]_{S_i} \leftarrow t[n]_i, d[n]_i$   $\triangleright$  reading synchronization
8:      $d[n]_{i_{relative}} \leftarrow d[n]_{S_i}, d[n]_{S_{i+1}}$   $\triangleright$  Relative displacement between every adjacent
        floors is calculated using Algorithm 4
9:      $IDR_i \leftarrow d[n]_{i_{relative}}$   $\triangleright$  Local  $IDR$  is calculated between every adjacent floors
        using Algorithm 4
10:   end for
11:    $IDR_b \leftarrow IDR_i$   $\triangleright$  Building  $IDR_b$  is calculated for The building using Algorithm 4
12:    $IO, LS, \text{ or } CP \leftarrow IDR_b$   $\triangleright$  A classification status is given to the building using
        FEMA standards
13: end for
```

On the other side, a cloud server was built for implementing all the signal processing needed for structural health assessment. Then the resultant building damage state along with location information are sent to the building health database. Finally, the resultant classifications are visualized using a detailed interactive map including buildings tagged with the most likely structural health status. The system flowchart is presented in Figure 2.9.

2.5 Initial system Experimental Validation

Several tests were conducted to determine the phone's ability to track phone displacement. A few more experiments were done in which different features were added to the system to test for improvement. The experiments were repeated for durations ranging from 5 to 30 seconds.

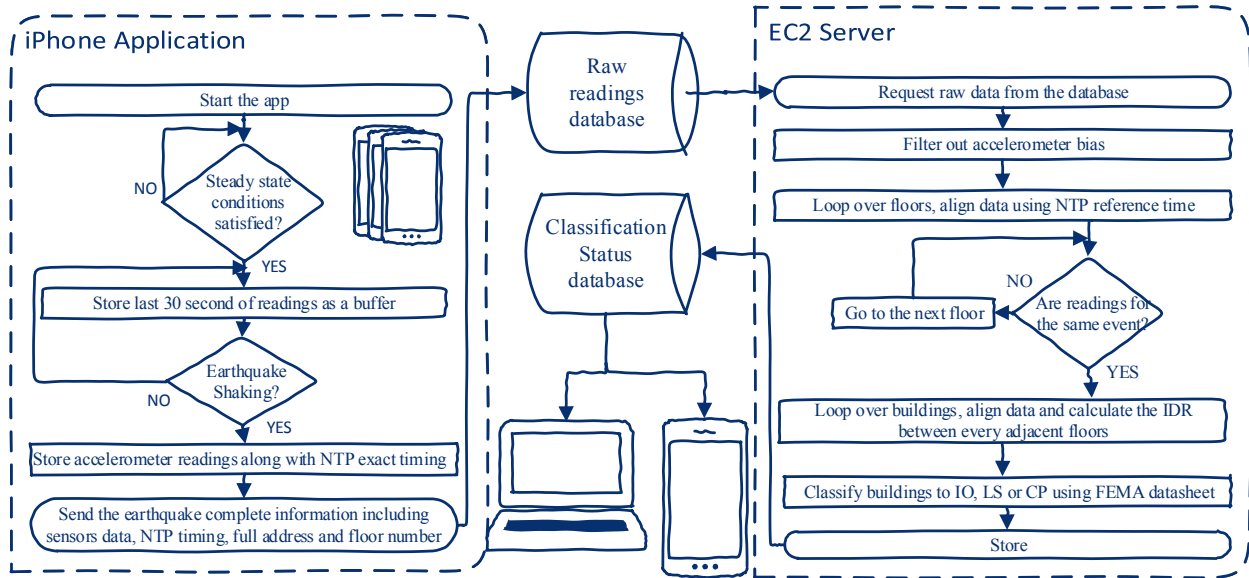


Figure 2.9: System Flowchart. The left hand side shows the mobile-phone application modes. The right hand side describes the signal processing of received phone acceleration signals.

Case I: At Rest

The first experiment conducted determines the effect that pure phone accelerometer noise has on the calculation of the relative displacement between two non-moving floors containing one device each. The two devices are triggered manually and left at rest for the whole experiment period. Ideally, the resultant relative displacement should be zero. However, the noise from phone accelerometer accumulated rapidly due to double integration. This error increased sharply as the the duration of the recorded event increased.

Case II: Using Mobile-Phone’s Internal Clock for Synchronization

Relying on the phone’s internal clock slightly enlarges the error in the IDR calculation. As explained in section 2.3 the best available option for indoor synchronization is using NTP as a common reference for all devices in the system. Figure 2.10 displays the average of the repeated full system tests relying on the mobile-phone’s internal clocks for data alignment.

The IDR calculation error in the system in the case of using the internal clock was larger than the case of using NTP time.

Case III: Identical Motion with NTP Synchronization

The last test applies an identical shaking motion to the two phones. The two devices are both bonded to a horizontal shaking slider. Ideally, they should get triggered at the same time and record the same acceleration. Additionally, since both phones are attached together, their relative displacement should be perfect zero. Consequently, any measured relative displacement is due to several other factors such as: trigger delay, amplitude-dependent accelerometer noise in addition to the accelerometer noise. As shown in Figure 2.10, the error is still tolerable for short durations (roughly 3 *cm* for periods shorter than 10 seconds).

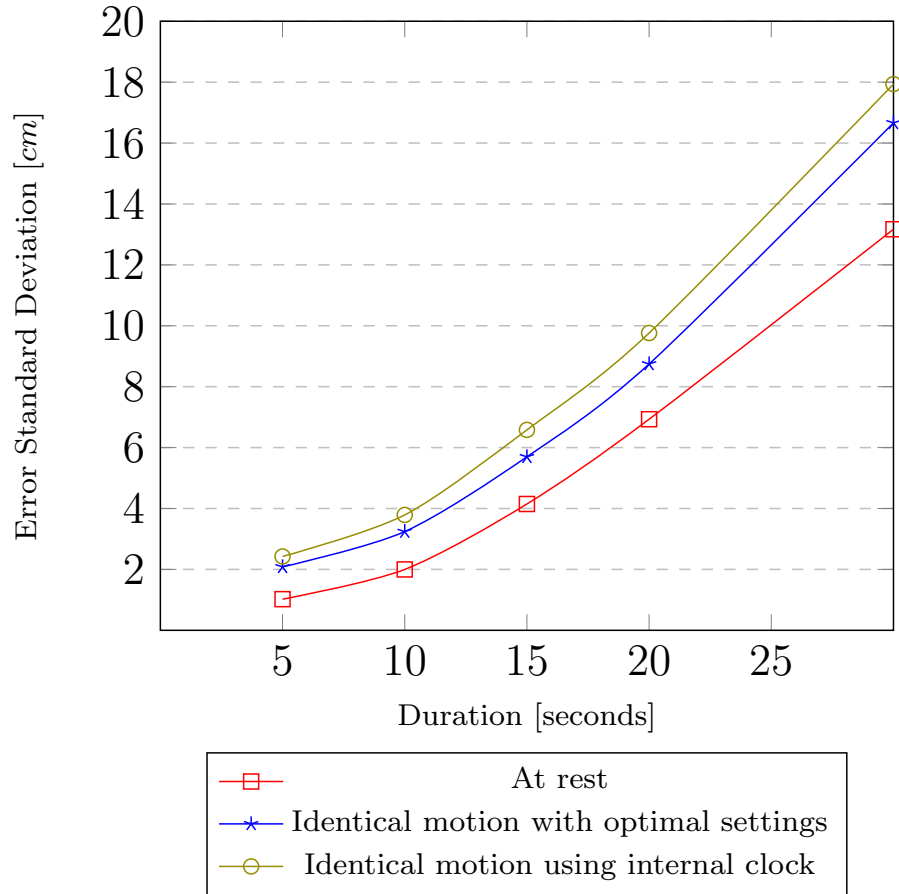


Figure 2.10: Error in IDR Using Smart-phone Accelerometer. Different settings and features were tested.

2.6 Conclusion

A smartphone accelerometer-based post-earthquake automated assessment system was built using client-server architecture. For the client side, an iPhone application was designed for earthquake detection. Once the earthquake is detected, the application saves the accelerations of the shaking. When the recording is finished, they are sent to the raw readings database which is used to register the unprocessed sensors readings, NTP timing and location details. On the other side, a cloud server was built for implementing all the signal processing needed for structural health assessment. Then the resultant building damage

state along with location information are sent to the building health database. Finally, the resultant classifications are visualized using a detailed interactive map including buildings tagged with the most likely structural health status.

To validate the feasibility of the system for structural health assessment, shake-table experiments were conducted showing a moderate accuracy in estimating the inter-story drifts. Next, methods to build on the proposed system to improve accuracy is presented in the following chapters.

Chapter 3

Vision-based Monitoring

Although smartphone accelerometers have been proven to detect earthquake shaking [40, 41, 42, 28, 22, 43, 29], estimating displacement from acceleration is vulnerable to error due to the double integration process, which amplifies low-frequency noise to undesired limits [44, 45]. An option to improve the accuracy of these accelerometers is to use the phone's camera, since it can measure displacement directly without the need for a double integration process. This technique proposes using the internal accelerometers of smartphones within a building to detect an earthquake, which then trigger the use of the smartphone's cameras in order to track the movement of the floors. The movement captured by a smartphone camera facing the ceiling of an upper floor actually shows the inter-story drift. An advantageous feature of using smartphones is that they have both front and back cameras, which makes it possible to use whichever camera is facing the ceiling. Since there is no control over the distance between the camera and the ceiling, the proposed system uses the smartphone accelerometer to estimate that distance, as discussed in details in chapter 4.

The remainder of the chapter is organized as follows. Section 3.1 presents the use vision-based techniques in previously developed SHM Systems. Section 3.2 presents development of

the proposed vision-based approach and the associated video processing. Section 3.3 reviews the experimental setup and validation of the vision-based tracking technique. Finally, the conclusion is drawn in section 3.4.

3.1 The use of Vision-based Techniques in SHM

Lately, vision-based structural health monitoring has gained traction due to the high accuracy afforded by directly measuring the displacement of structures during earthquake events instead of estimating displacement using accelerometer readings, which may not be accurate due to a bias in low-frequency contents. [21] developed a structural health monitoring (SHM) system by installing action cameras onto a beam that is 22m away from a bridge to capture the movement of the bridge in response to crossing trucks in order to assess the structural integrity, taking into account the weight of the truck. In another work, [22] used a smart-phone camera that was fixed a few centimeters away from a suspension-bridge's cable to measure the resonance frequency, as well as, its horizontal and vertical movement. The purpose of these two projects was to estimate the structural damage in non-earthquake scenarios.

The use of SHM systems that was designed to be used in non-earthquake scenarios faces three major challenges when used to estimate damage due to earthquake events. First, they require the camera to be stationary during the recording of the event, which is not achievable during earthquakes. Second, they are not feasible for large scale deployment due to the cost of installation and wired/wireless connection. Third, they are installed outdoors making them sensitive to weather conditions and visibility range (i.e. not feasible for dark or foggy conditions). Unlike other vision-based systems, our proposed system uses citizen owned smart-phone cameras to track the movement of structures during the earthquake, from

within the structure itself. The system analyzes collected videos to calculate the horizontal movements of structures in the targeted area in order to infer their state.

3.2 The Development of Vision-based SHM Method

The proposed vision-based SHM method uses several image processing techniques.

3.2.1 Feature Extraction

The previously developed vision-based SHM systems [22, 25] use a target that needs to be attached to the monitored structure, which complicates large-scale deployment. Additionally, the system in [21] requires manually choosing a region of interest (ROI) in the camera view to be tracked. In the proposed approach, the algorithm tracks identifiable objects on the ceiling. For example, in an office setting, ceiling tiles could be targeted, whereas in a home setting, recessed light fixtures could be targets. Thus, to simplify deployment, the proposed system uses an automated algorithm to detect the main features of the ceiling and uses them as targets for image processing feature extraction techniques. The system uses features from the accelerated segment test (FAST) method [46], which is a robust and computationally efficient sharp corner detector. The FAST corner detector uses a 16-pixel circle to identify whether a candidate point p is a corner or not. The point p is classified as a corner if a set of 12 contiguous pixels in the circle are all brighter (or darker) than the intensity of the candidate pixel p , plus (or minus) a threshold. The color videos captured are converted to grayscale to reduce computational complexity. Figure 3.1 shows a typical frame displaying what a smartphone may capture in an office setting. The red crosses in the image are the features detected using the FAST algorithm. Shake table experiments of standard office tile ceilings show minimal deformation at high levels of shaking [47]. Although some tiles fell

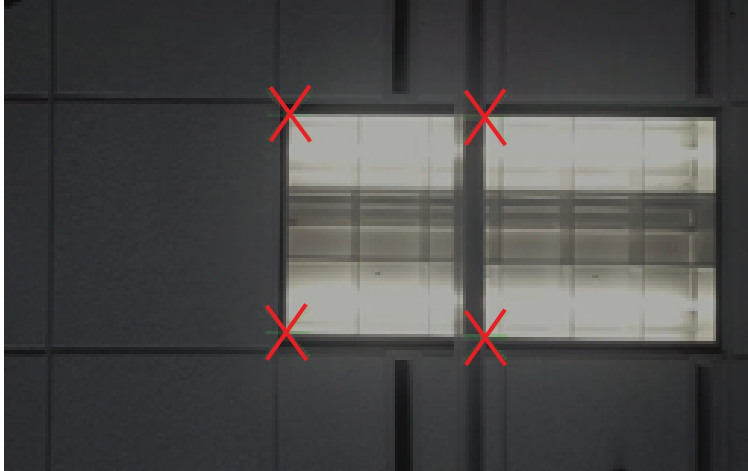


Figure 3.1: Image of a typical office ceiling. Red crosses in the image are the detected features from the accelerated segment test (FAST) algorithm.

during the shake table tests, the main beams that holds the ceiling tiles showed minimal damage [47].

3.2.2 Feature Tracking

Once the main features are detected, the Kanade–Lucas–Tomasi (KLT) algorithm [48] is used to track changes in the location of the detected features frame by frame for the duration of the earthquake. The KLT algorithm uses spatial intensity information and a pyramidal scheme to direct the search for the tracked feature.

3.2.3 Scaling Factor (SF)

One of the most challenging steps is to identify a scaling factor ($mm/pixel$) to convert the extracted displacement from pixels to displacement units (i.e. mm). In our experiments, the scaling factor is calculated using the reading of the phone’s internal accelerometer to estimate the scaling factor since it is already pre-calibrated by the manufacturer to engineering units (i.e. mm/s^2), which is presented in details in chapter 4.

A summary of the vision-based structural health monitoring algorithm is presented in Figure 3.2.

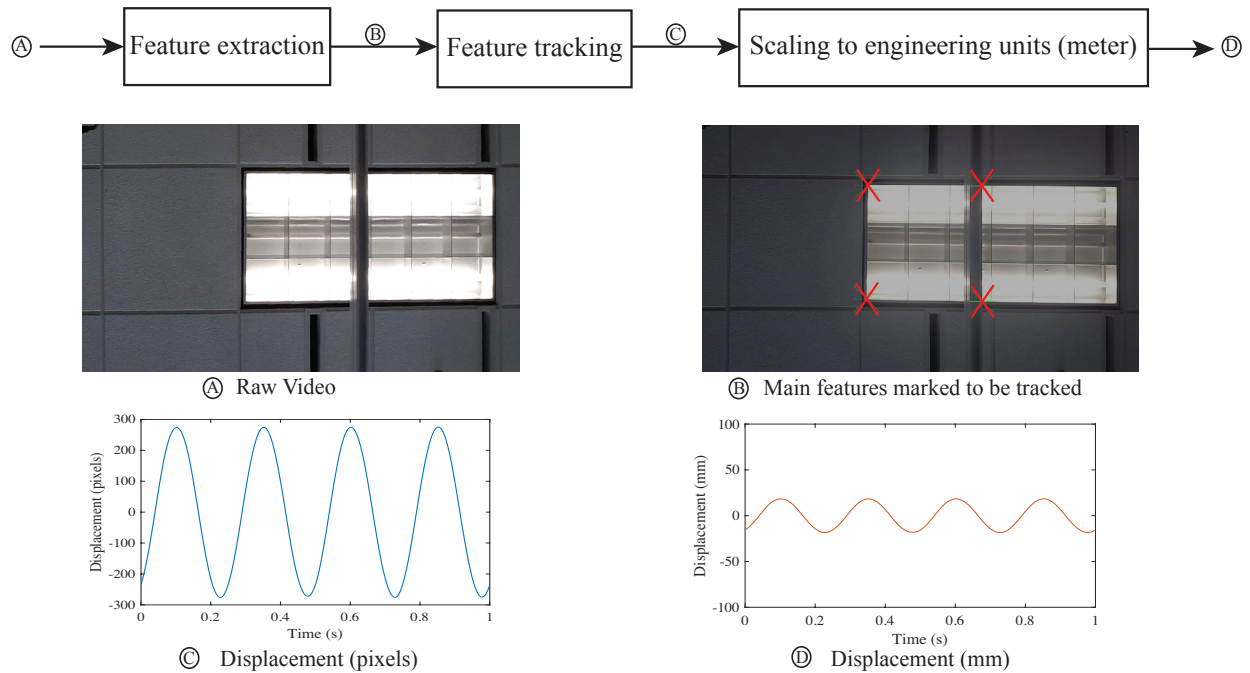


Figure 3.2: Vision-based Structural Health Monitoring algorithm Process

3.3 Vision-based Tracking Experimental Setup and Results

A series of experiments of floor movement during an earthquake were conducted using a shake table. Different shaking frequencies and amplitudes were used to simulate real earthquake shaking. The shaking table is laid horizontally on the ground and a smart phone is attached to the top of the shaking table as shown in Figure 3.3. When the shaking table starts moving, the smart-phone application begins recording data and video of the ceiling. After the shaking ends, the proposed algorithm analyzes the video and extracts movement the phone experience since the ceiling is not moving (what is being measured is, in fact, the

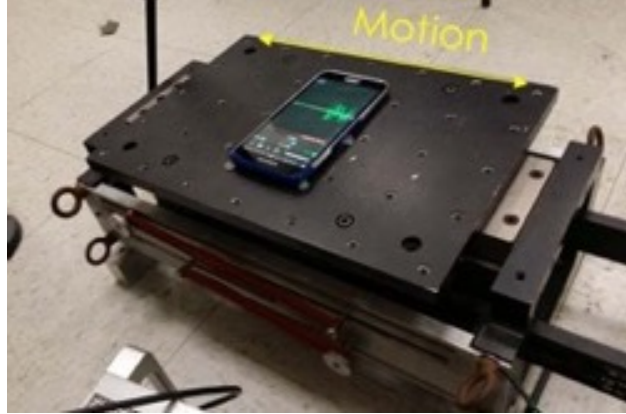


Figure 3.3: Shake table setup used in the experiment

relative displacement between the phone and the ceiling). A seismic-grade accelerometer is attached to the shake table as a reference to determine the accuracy of the proposed vision-based approach.

The focus of this experiment is to test the feasibility of using the camera for displacement estimation, rather than the accuracy in finding the Scaling (SF), which is discussed in details in chapter 4. For that reason, the scaling factor (SF) is calculated manually using the technique discussed in [21].

The first shaking experiment was performed using a 4 Hz 36 mm peak-to-peak sinusoidal shaking for 30 seconds. The mobile-phone app successfully triggered and captured the movement of the shaking table, while targeting ceiling tiles as anchor points. Figure 3.4 shows the horizontal displacement of the smart-phone as measured using the proposed vision-based tracking technique in red. The displacement distilled from the reference accelerometer is plotted in blue showing great tracking. The deviation in estimating the displacement using the proposed algorithm is presented in Figure 3.5. One cycle of the displacement is presented in Figure 3.6 showing an agreement with slight variation between the estimated displacement of the proposed tracking technique and the reference. The RMS of the error of the proposed vision-based method was 0.16 mm . The vision-based tracking method was tested using dif-

Table 3.1: Sinusoidal shaking of different amplitudes and frequencies

Shaking Frequency	Peak-to-peak Shaking Amplitude	RMS of the error
4 Hz	36.8 mm	0.156 mm
5 Hz	26.8 mm	0.139 mm
6 Hz	19.7 mm	0.121 mm
7 Hz	14.6 mm	0.097 mm

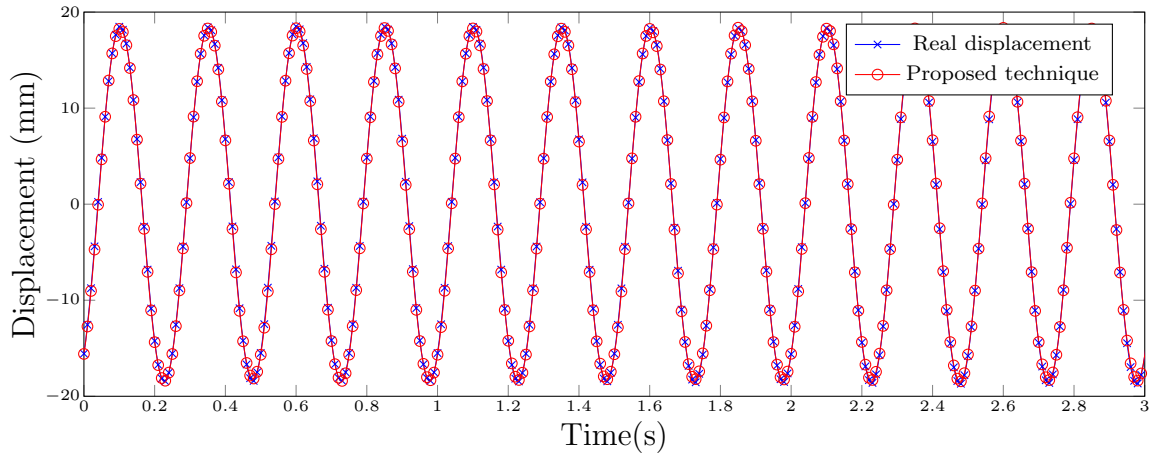


Figure 3.4: Displacement extracted using proposed camera based SHM approach in red, and reference in blue

ferent scenarios of shaking amplitudes and frequencies. TABLE 3.1 lists the parameters of the shaking signals as well as the RMS of the error in each experiment.

After the relative displacement was estimated for adjacent floors in the building, the IDR value is calculated using (1.1). Buildings are then categorized into IO, LS or CP using FEMA standards [2]. For a standard 4 m floor height building, an error of 0.16 mm in displacement calculation will result in 4e-5% IDR error, which is negligible compared to the classification limits. The effect of displacement estimation error to the status classification has been exhaustively studied in Section 4.4 and in [44].

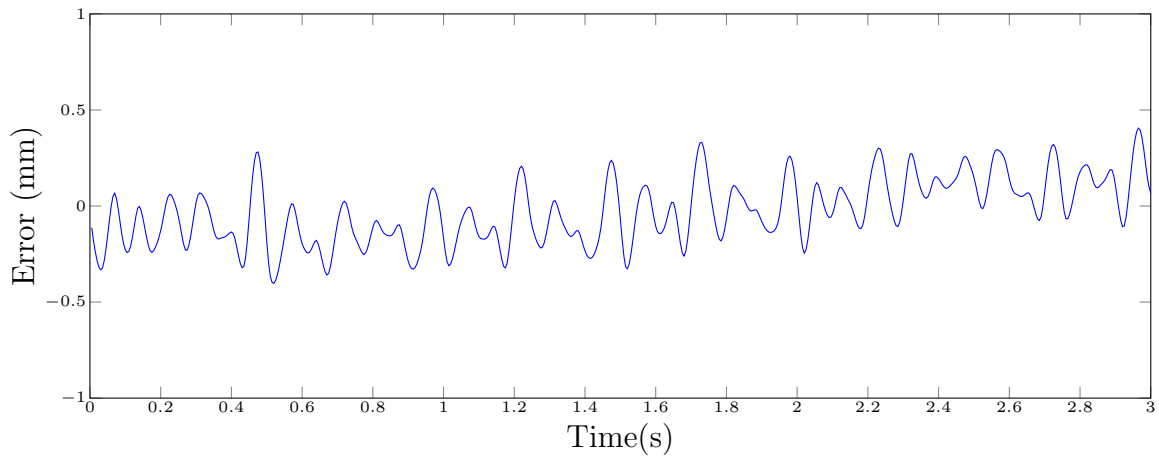


Figure 3.5: Error in displacement extracted using proposed camera based SHM approach

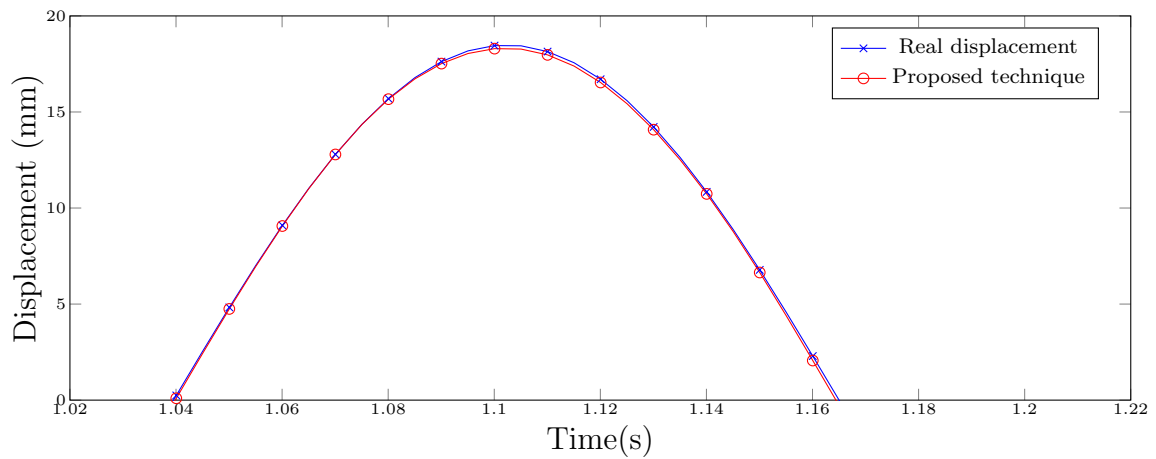


Figure 3.6: One cycle of displacement extracted using our camera based SHM approach in red, and from the reference in blue

3.4 Conclusion

A post-disaster vision-based structural health monitoring methodology has been developed utilizing cameras of smart-phones. The smart-phone's accelerometers were used to detect earthquakes and the cameras were used to track the movements of the upper floor during earthquake shaking. This method avoids the necessity for an off-structure reference point, in addition to making it insensitive to weather conditions and visibility range. To validate the method feasibility, shaking table experiments were conducted. Sub-millimeter accuracy was achieved using the proposed vision-based SHM method which is considered to be ultra-high accuracy in structural monitoring standards and outperforms accelerometer based SHM systems. The calibration of the smartphone camera using the accelerometer readings is discussed in the next chapter, which remove the need of manually finding the scaling factor and easing the path for large scale deployment.

Chapter 4

Multi-sensory System (Version 2.0)

This system proposes using the internal accelerometers of smartphones within a building to detect an earthquake, which then trigger the use of the smartphone's cameras in order to track the movement of the floors. Since there is no control over the distance between the camera and the ceiling, the proposed system uses the smartphone accelerometer to estimate that distance.

The remainder of the chapter is organized as follows: Section 4.1 presents the structural damage classification process, including video processing, camera self-calibration, and the phone's sliding detection algorithms. The architecture of the proposed community-based SHM network is detailed in section 4.2, including the smartphone application and the cloud-based server. Section 4.3 reviews the shake table experimental setup and validation. The performance of the proposed SHM system in identifying structural damage is presented and compared with other recently developed SHM systems in section 4.4. Finally, the conclusions are drawn in section 4.5.

4.1 Structural Health Classification Process

As mentioned earlier, this system proposes using the internal accelerometers of smartphones within a building to detect an earthquake, which then trigger the use of the smartphone's cameras in order to track the movement of the floors. The movement captured by a smartphone camera facing the ceiling of an upper floor actually shows the inter-story drift. The image processing techniques required to estimate the movement of floors using video records is discussed in section 4.1.1. Since there is no control over the distance between the camera and the ceiling, the proposed system uses the smartphone accelerometer to estimate that distance, as discussed in Section 4.1.3. Additionally, because smartphones are not mounted to the structure, sliding of the phone over the surface it is resting on is possible; sliding detection and how to mitigate its effect are discussed in section 4.1.2.

4.1.1 Vision Algorithm

In the proposed approach, the algorithm uses cameras of smart-phone that are laid horizontally on tables to track identifiable objects on the ceiling. For example, in an office setting, ceiling tiles could be targeted, whereas in a home setting, recessed light fixtures could be targets. Thus, to simplify deployment, the proposed system uses an automated algorithm to detect the main features of the ceiling and uses them as targets for image processing feature extraction techniques. The system uses features from the accelerated segment test (FAST) method [46], which is a robust and computationally efficient sharp corner detector. Figure 3.1 shows a typical frame displaying what a smartphone may capture in an office setting. The red crosses in the image are the features detected using the FAST algorithm. Once the main features are detected, the Kanade–Lucas–Tomasi (KLT) algorithm [48] is used to track changes in the location of the detected features frame by frame for the duration of the earthquake. Section 3.2 details the video processing techniques used by the proposed system.

4.1.2 Smartphone Sliding Detection

Smartphones may slide during an earthquake if they are placed on a smooth enough surface. This issue has been addressed in prior work [49, 50, 51], where a sliding detection algorithm was developed that detects whether the phone is sliding while recording an event, in addition to the time window of the sliding. The algorithm is an accelerometer-based stick-slip motion classification framework based on a machine learning approach. The algorithm was experimentally tested using a series of shake table experiments under different shaking scenarios. Additionally, the proposed algorithm has been experimentally proven to detect sliding of the table on which the smartphone was placed. Consequently, segments with sliding can be rejected.

To minimize sliding leading to rejected readings, several guidelines are recommended for users and building managers, especially in earthquake-prone areas. Smart-phone cases with high kinetic coefficients of friction (KCOF), such as leather or silicone cases, are recommended. In [50], the sliding of a smartphone without a case (KCOF = 0.164), with a leather case (KCOF = 0.237), and with a silicone case (KCOF = 0.508) was tested using a shake-table, showing a better sticking performance with higher KCOF. Additionally, workplaces and building owners in earthquake-prone areas are recommended to install in-ground mounted tables and workstations with high KCOF surface materials, such as laminate [52] or rough-sawn wood tabletops [53], to minimize the number of rejected readings due to sliding. Having a high KCOF surfaces can be achieved by applying a high KCOF coating to existing tables and workstations [54]. Moreover, workplaces and building owners are recommended to incentivize employees and residents to use the system to enhance safety management in the case of an earthquake. Having a high enough number of active devices on each floor increases the likelihood of having valid readings in each floor.

It is possible that some floors may not have valid readings of their movement due to sliding or unavailability of active devices. In this case, it is reasonable to indirectly estimate the movement based on the displacements of adjacent floors. Conventionally, motions of the noninstrumented floors are estimated by an interpolation procedure [55], e.g., by using a piece-wise cubic polynomial interpolation (PWCPI) procedure.

4.1.3 Camera Self-Calibration

One of the most challenging issues is converting the extracted displacement from pixels to displacement units, i.e., mm . In the proposed system, calibration is performed automatically using readings from the phone's internal accelerometer, which was already pre-calibrated by the manufacturer. The scaling factor k is defined as the gain between the pixel displacement (pixel inter-story drift) inferred from the camera readings and the physical mm displacement (inter-story drift), which is defined as:

$$\mathbf{s} = \frac{1}{k} \check{\mathbf{s}}_p, \quad (4.1)$$

where \mathbf{s} is a column vector of the mm-displacement samples for the observation instance $m \in [0, M)$, $\mathbf{s} = \begin{bmatrix} s_0 & s_1 & \dots & s_{M-1} \end{bmatrix}^T$; $\check{\mathbf{s}}_p$ is a vector of the pixel-displacement samples, $\check{\mathbf{s}}_p = \begin{bmatrix} \check{s}_{p0} & \check{s}_{p1} & \dots & \check{s}_{p_{M-1}} \end{bmatrix}^T$.

However, since converting acceleration to displacement by double integration amplifies low-frequency noise, the system directly calculates the scaling factor using accelerations. The system converts the camera-inferred pixel-displacement ($\check{\mathbf{s}}_p$) to pixel-acceleration ($\check{\mathbf{a}}_p$) as:

$$\check{\mathbf{a}}_p = \mathbf{H} \check{\mathbf{s}}_p, \quad (4.2)$$

where the square matrix \mathbf{H} is the centered difference approximation of the second derivative of a column vector [56], which is defined as:

$$\mathbf{H} = f_s^2 \begin{bmatrix} 1 & -2 & 1 & 0 & \cdots \\ 0 & 1 & -2 & 1 & \cdots \\ 0 & 0 & 1 & -2 & \cdots \\ 0 & 0 & 0 & 1 & \cdots \\ \vdots & \vdots & \vdots & \vdots & \ddots \end{bmatrix},$$

where f_s is the sampling rate. Since k is a constant, Equation (4.1) can be rewritten using Equation (4.2) as:

$$\check{\mathbf{a}} = \frac{1}{k} \check{\mathbf{a}}_p,$$

where $\check{\mathbf{a}}$ is a column vector of the mm-acceleration samples for the observation instance $m \in [0, M)$, $\check{\mathbf{a}} = \left[\check{a}_0 \quad \check{a}_1 \quad \cdots \quad \check{a}_{M-1} \right]^T$; $\check{\mathbf{a}}_p$ is a vector of the pixel-acceleration samples, $\check{\mathbf{a}}_p = \left[\check{a}_{p0} \quad \check{a}_{p1} \quad \cdots \quad \check{a}_{pM-1} \right]^T$.

$\check{\mathbf{a}}_p$ is found using the camera-inferred pixel-displacement using Equation (4.2). $\check{\mathbf{a}}$, the relative acceleration between adjacent floors, is found by subtracting raw accelerometer readings from smartphones on consecutive floors as:

$$\check{\mathbf{a}} = \check{\mathbf{a}}_{a_i} - \check{\mathbf{a}}_{a_{i+1}}, \tag{4.3}$$

where $\check{\mathbf{a}}_{a_i}$ is the (absolute) acceleration measured by the internal accelerometer of the phone on floor i .

Then, k can be found as:

$$k = \sqrt{\frac{\sum_M (\ddot{a}_{pm})^2}{\sum_M (\ddot{a}_m)^2}}, \quad (4.4)$$

where $m \in [0, M)$ and 0 represent the beginning of the earthquake.

After finding k , the inter-story drift \mathbf{s} is calculated using Equation (4.1). After that, **IDR**, which is a column vector of the IDR samples for the observation instance $m \in [0, M)$, is calculated as:

$$\mathbf{IDR} = \frac{\mathbf{s}}{h}, \quad (4.5)$$

where h is the floor height in mm . Finally, a class is assigned to the building by comparing the peak **IDR** with the Federal Emergency Management Agency (FEMA) reference values shown in Table 1.2.

4.1.4 Signal Preconditioning

To fuse readings from both the accelerometer and the camera, the following issues have to be considered:

- Typically, the sampling rates are different: a camera samples at rates that are typically 30 frames per second (fps), whereas the sampling rate of the accelerometer is typically 100 Hz .
- Practically, there might be a slight delay between the triggering of the camera versus that of the accelerometer.

- Smartphones on different floors do not necessarily have the same directional alignment, for example, one might be positioned heading north while the other is positioned heading east.

Figure 4.1 highlights the approach proposed to address these issues. First, the sampling frequency is unified by resampling the reading with a higher sampling rate. Second, the cross-correlation between the camera reading and the accelerometer reading is used to find the lag that maximizes the cross-correlation. Then, readings are aligned by time-shifting according to the lag time. Third, the smartphone’s internal magnetometer is used to align (rotate) the acceleration and the camera records towards the north.

4.1.5 Sensor Fusion Flow

Figure 4.1 presents the flow of the proposed building’s health classification algorithm. First, the accelerometer and camera records of smartphones that are within a given building are accessed. Second, the relative acceleration between adjacent floors is found by synchronizing readings using the network time protocol (NTP) time stamps attached to each acceleration reading, then subtracting the accelerometer reading of the smartphone on the upper floor from the reading of the one on the lower floor. Third, the vision algorithm discussed in Section 4.1.1 is applied to the camera records of each floor to infer the pixel inter-story drift (green block, Figure 4.1). Fourth, the scaling factor k is found using the self-calibration algorithm discussed in Section 4.1.3, preceded by the signal preconditioning mentioned in Section 4.1.4 (blue block, Figure 4.1). Fifth, the inter-story drift is found using Equation (4.1). Finally, the IDR is calculated using Equation (4.5) and a class is assigned to the building using the limits in Table 1.2. If there are multiple phones on the same floor, the scaling factor k is found for each smartphone’s readings individually; then the system averages the readings before finding the IDR. Therefore, the upper-floor’s displacement calculation is independent

of whether the smartphone is placed on a high or a low table. The processes discussed in this section are performed by the cloud server, which is explained in Section 4.2. Additionally, the details of the databases mentioned in Figure 4.1 are discussed in Section 4.2.

In summary, the proposed algorithm uses the readings of smartphones on two adjacent floors, i.e., accelerometer readings on the two floors, in addition to the camera records of the smartphone on the lower floor, to estimate the structural health of a given floor of a building. A network of smartphones on each floor of the building being monitored is needed; the scaling up of this network is discussed in Section 4.2.

4.2 Community-Based SHM Network

To achieve low-cost and large-scale deployment, the proposed system uses the network of smart devices that has already been deployed. The system was developed using a client-server architecture. The user application is used to detect earthquakes, store sensor data, and upload records to a cloud-based database. The server uses uploaded sensor records to estimate the severity of the damage to structures. The server then generates a disaster map that displays buildings tagged with their damage state.

4.2.1 Smartphone Application

Part of this work was the development of a mobile phone application that detects an earthquake and sends sensor readings to a centralized cloud computing server. When the app is installed, the user is asked to confirm the address and floor number; the app works silently in the background afterwards. The app becomes active to record earthquakes if steady-state conditions are satisfied, i.e., the smartphone has to be horizontally laid on a flat surface, such as a table, and stay stationary for at least 30 seconds. This steady state is needed to ex-

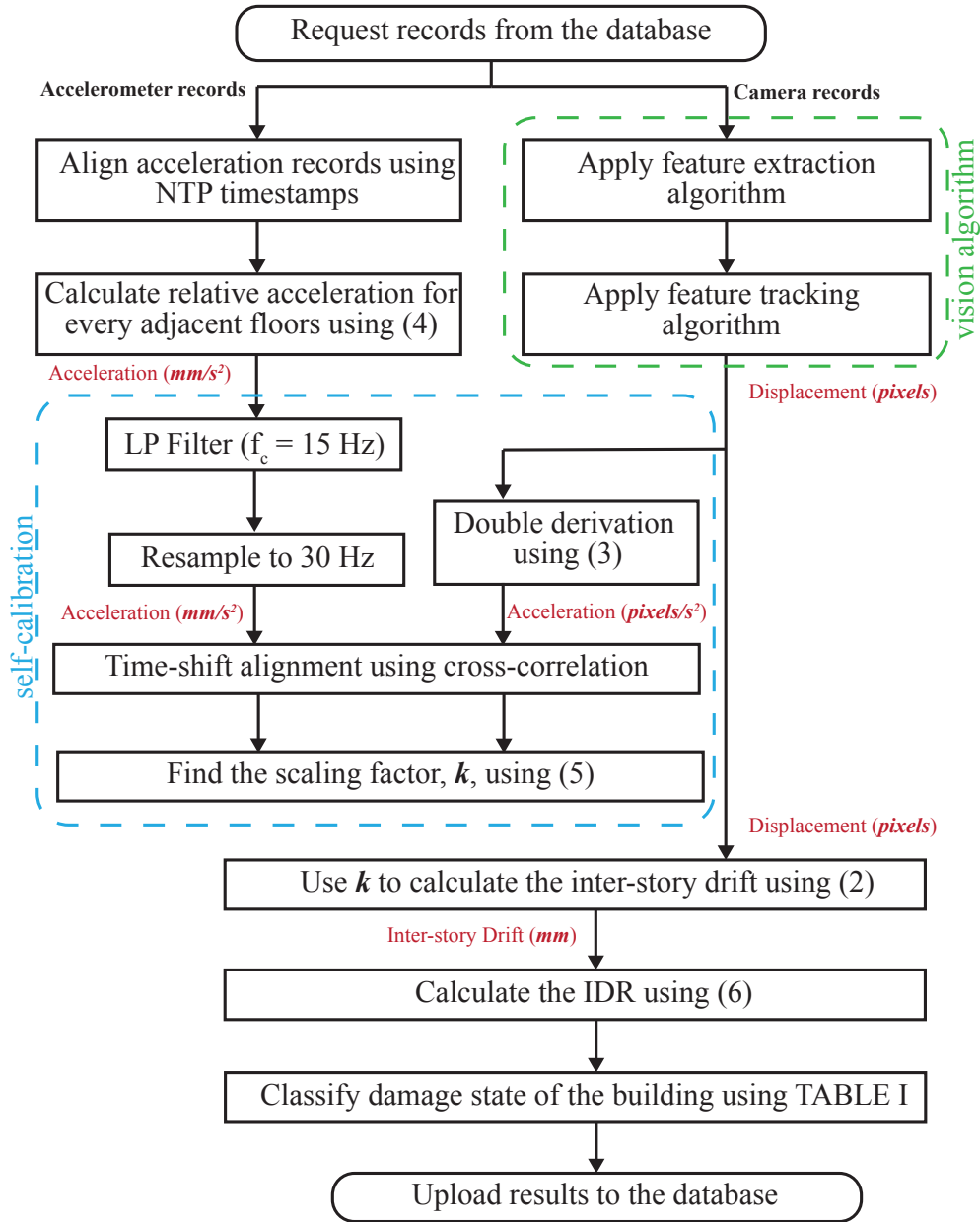


Figure 4.1: Overview of the structural health classification process used in the proposed multi-sensory structural health monitoring (SHM) system. The red labels on the arrows represent the quantity being measured and its units. The dashed-green block in the upper right highlights the vision algorithm, which obtains the camera records of the ceiling movement and outputs pixel inter-story drift data. The dashed-blue block in the middle (on the left) highlights the self-calibration algorithm preceded by signal preconditioning; this block obtains the inter-story acceleration and pixel inter-story drift and outputs the scaling factor k .

clude phones that might lead to inaccurate readings, such as phones held by users or placed in suitcases. The app starts recording sensor data as soon as an earthquake is detected, i.e., when the predetermined threshold ($0.1g$) has been crossed in the x–y direction. This technique was used in several seismic smartphone apps such as iShake [27] for earthquake detection because of its power efficiency. Then, the records are sent to the centralized cloud server.

A smartphone’s camera and accelerometer sampling rates are variables that are set by the application (app) developer. In the proposed system, the camera sampling rate is set to 30 fps, while the accelerometer samples at 100 Hz . Additionally, calculating relative displacements (IDR) requires millisecond accuracy for proper synchronization between devices. Therefore, a synchronization technique is required across phones to avoid clock drift. The proposed application uses network time protocol (NTP) timing to ensure that there is an accurate simultaneous reference for all devices [36]. An overview of how the app works is shown in Figure 4.2. Screenshots of the smartphone application are presented in Figure 4.3.

4.2.2 Cloud Server

Using a cloud server provides major advantages over using a standard server in terms of scalability, cost, and availability. The proposed system uses an Amazon web services (AWS) elastic compute cloud (EC2) as the basis for all computations and processes needed, which are described in Section 4.1.

4.2.3 Database

The system uses the cloud-based MySQL database because of its ability to store and organize thousands of readings that can be recalled as and when required. The system consists of

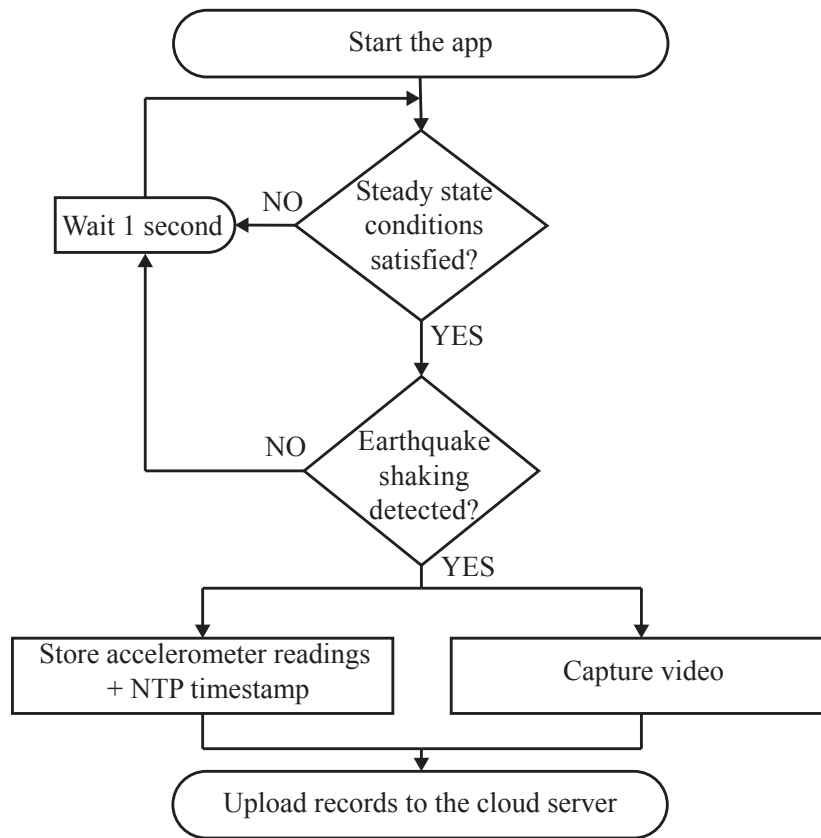


Figure 4.2: The smartphone application process. Seismic sensing is performed silently in the background.



Figure 4.3: Screenshots of the smartphone application. The seismic sensing is performed silently in the background. The building’s structural safety status is fed back to the user in the form of a disaster map.

three different databases. One database is used to store raw data received from the app, along with location information. Another database is used to store the resulting damage state for each building, along with the time and date of the incident (earthquake). The last database contains checkpoints for system debugging. Raw sensor readings can be used in other applications, such as constructing a higher-resolution ground shaking map [30, 31, 32]. Additionally, acceleration readings of floors can be used for nonstructural damage detection, such as in [15] and [16] where the acceleration of a given floor is used in the damage prediction of nonstructural elements.

4.2.4 Visualization

Buildings, along with their structural health status, are listed on the system’s website, which is also hosted by the AWS server. In addition, the website includes a map of the buildings

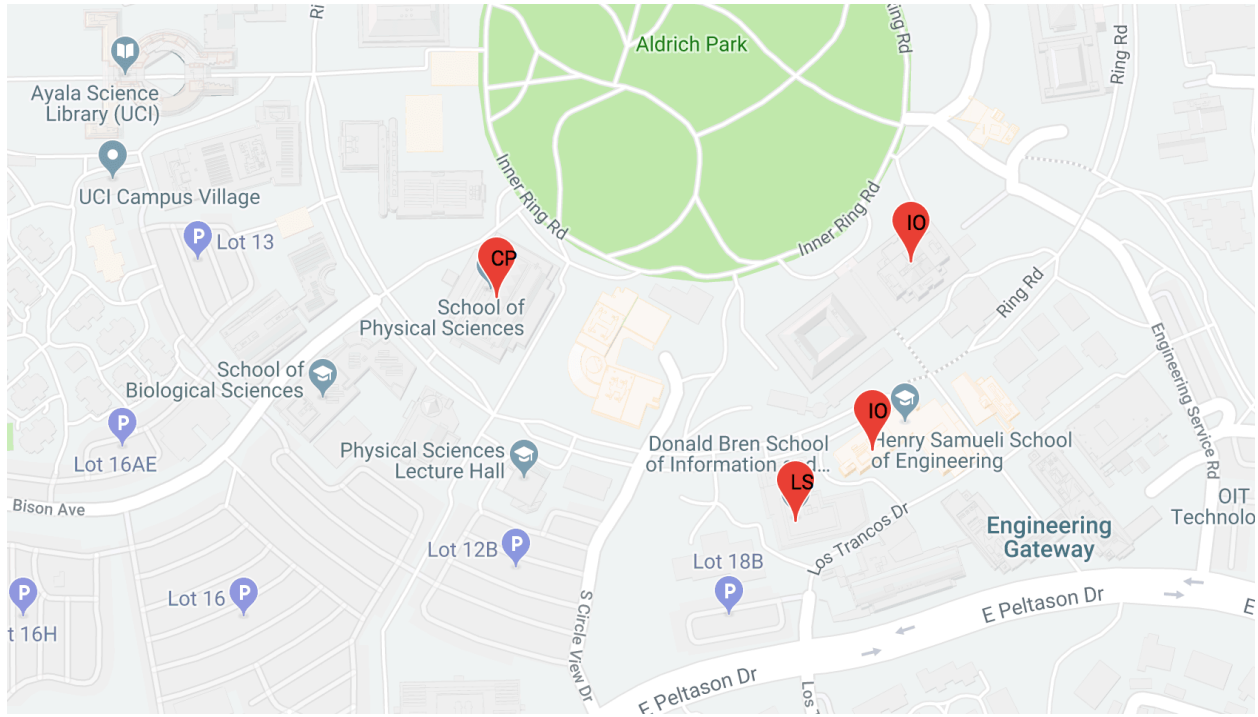


Figure 4.4: Website screenshot. A detailed map is shown containing buildings tagged with their most likely structural health status.

tagged with their structural health state, thus making it easier for the public to check buildings in the aftermath of an earthquake. A screenshot of the web page is shown in Figure 4.4.

Figure 4.5 shows the flow of the system from detecting an earthquake to creating the disaster map.

4.3 Shake Table Validation

To validate the proposed SHM system, a series of experiments were performed. This section reports the experimental setup, procedures, and results. A seismic shake table was used to test the system's ability to estimate the inter-story drift of a building under dynamic shaking

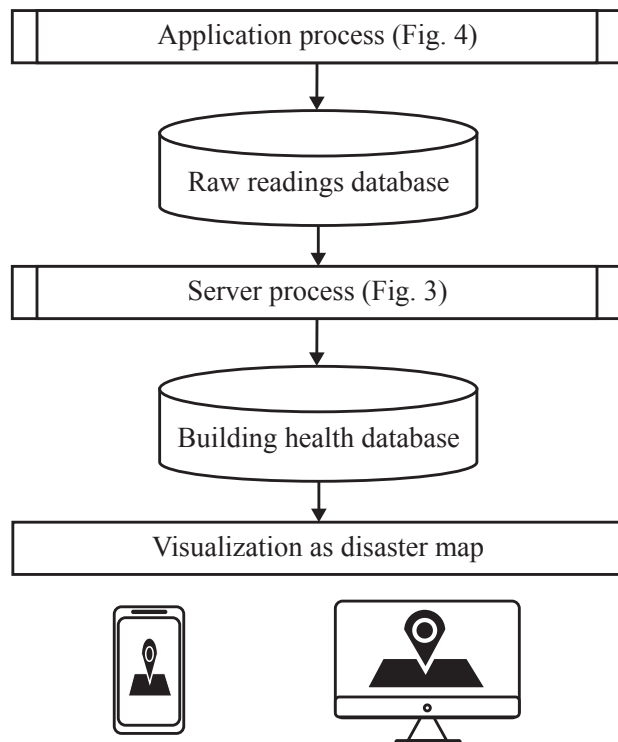


Figure 4.5: The proposed community-based SHM network layout. The smartphone app process is explained in Section 4.2.1 and Figure 4.2. The server process is discussed in Section 4.1 and Figure 4.1. The disaster map is visualized in Figure 4.3 and Figure 4.4.

Table 4.1: The tested smartphones’ technical specifications.

	SMG900T	SMG920V
Operating system	Android V5.1.1	Android V7
Camera sensor	ISOCELL S5K2P2 [59]	ISOCELL S5K2L1 [60]
Video resolution	1080p	1080p
Accelerometer chip	InvenSense MPU-6050 [61]	InvenSense MPU-6500 [62]
Commercial name	Samsung Galaxy S5	Samsung Galaxy S6

(e.g., an earthquake). Shake table validation is the testing methodology used in most SHM studies [10, 20, 22].

Three different smartphones were used in the experiments: SMG900T and two different SMG920V devices. Table 4.1 lists the operating system, the commercial name, the camera sensor manufacturer, the video resolution, and the accelerometer chip manufacturer of the devices used in the experiments. A seismic-grade accelerometer (PCB Piezotronics Model393C [1]) was used as a reference. The smartphones and the reference were attached to the shaking table, as shown in Figure 4.6. The shake table was used to perform 4 different experiments; in each of the experiments, a sinusoidal signal with a frequency of 4, 5, 6, or 7 Hz was used to excite the shake table. This specific range of frequency was chosen based on many previous research studies reporting that both the strong motion of earthquakes and the natural frequency of buildings have a frequency of less than 10 Hz [57, 58]. The laboratory in which the experiment was conducted was chosen to have a ceiling that is typically found in office settings, as shown in Figure 3.1. Since smartphones on a given floor do not necessarily have the same distance from the ceiling, the scaling factor algorithm is applied for each smartphone’s readings individually.



Figure 4.6: Shake table experimental setup. The reference accelerometer (Model393C [1]) was attached to the shake table, which is shown on the right hand side.

The sampling rates for the sensors used in the experiments were: 30 fps for the smartphone camera, 100 Hz for the smartphone accelerometer, and 20 kHz for the reference accelerometer. The procedures for each experiment were as follows: first, the displacement was calculated as described in Section 4.1.5 and summarized in Figure 4.1; in the performed experiments, the accelerometer readings were considered as the relative acceleration since the ceiling was not moving; second, the estimated displacement was up-sampled using a cubical interpolation of the reference sampling rate; third, the reference displacement was inferred by double integrating the reference acceleration; fourth, the reference displacement was time-shifted by the lag that maximizes the cross-correlation; finally, errors were found by subtraction. The experimental procedure is summarized in Figure 4.7.

Figure 4.8 presents the estimated drifts using the proposed system for different devices for different experiments. Ground truth drifts are included for comparison. The inter-story drift estimated using the SHM system (\mathbf{s}) can be expressed as:

$$\mathbf{s} = \mathbf{s}_t + \mathbf{e}, \quad (4.6)$$

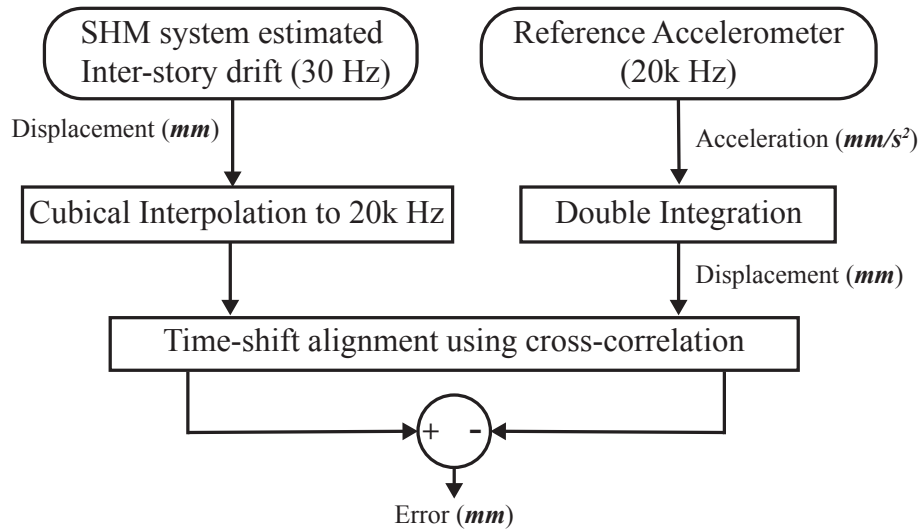


Figure 4.7: The procedures followed in each experiment.

where \mathbf{s}_t is the true inter-story drift and \mathbf{e} is the error, which is approximated as a zero-mean Gaussian distribution with variance σ_e^2 , $\mathbf{e} \sim \mathcal{N}(0, \sigma_e^2)$.

Table 4.2 lists the different experimental parameters and accuracy achieved by each phone described by the standard deviation of the error (σ_e). Several studies [33, 34, 20] have reported the suggested SHM system accuracy as 0.002 IDR (8 mm); the proposed system consistently achieved sub-millimeter (0.0002 IDR) accuracy and is thus suitable for SHM purposes.

4.4 System Performance

This section studies the overall performance of the proposed SHM system and compare it to other currently available SHM systems. The performance of the SHM system was evaluated by calculating the system's probability of classification error (p_e) using the formula derived

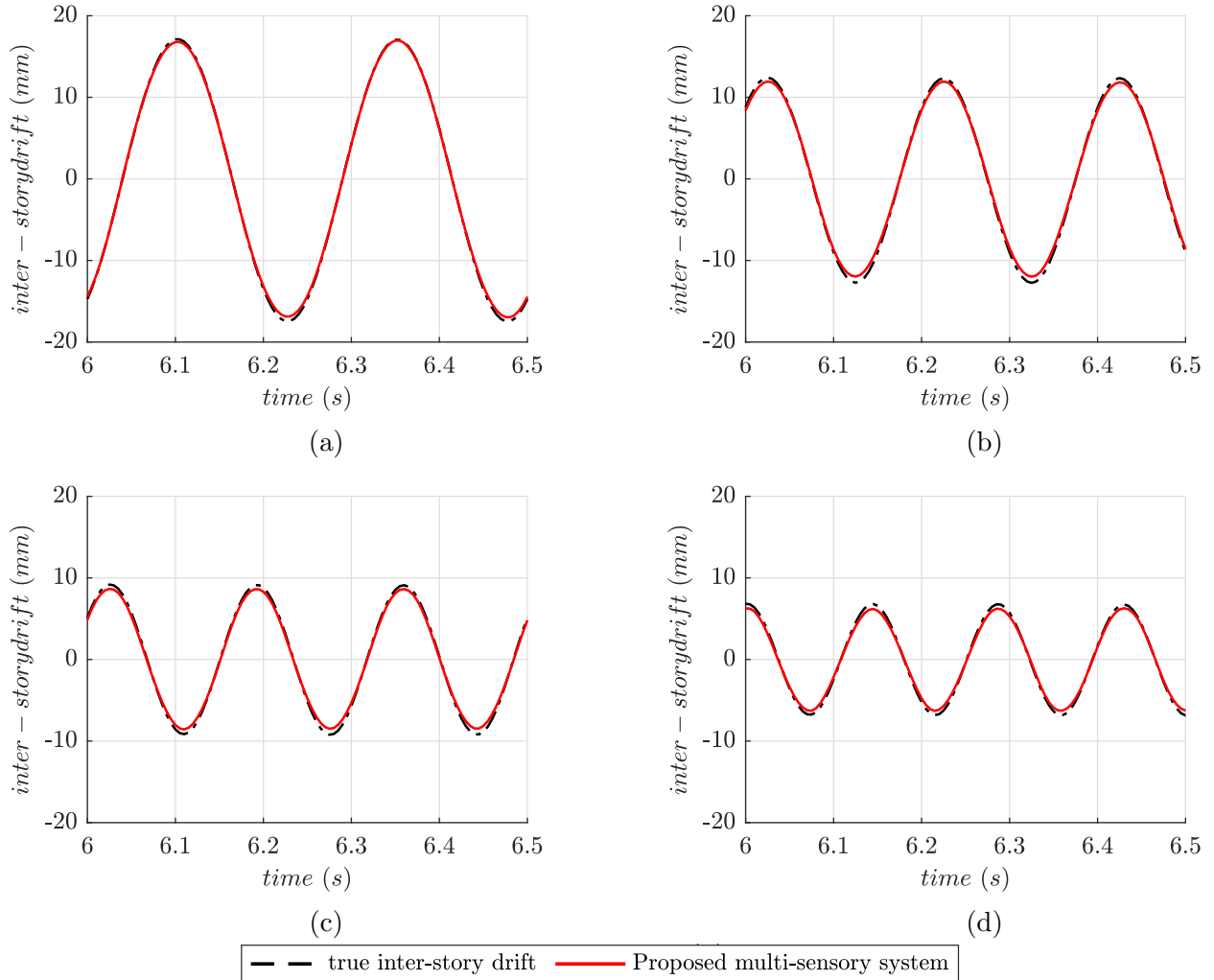


Figure 4.8: True inter-story drifts (dashed black lines) plotted with the drift estimated using the proposed algorithm (solid red lines). The drifts estimated using the proposed algorithm show good agreement with the ground truth. The smartphone model and excitation signal for each experiment were: (a) SMG900T with a sinusoidal excitation of 34.7 mm peak-to-peak amplitude and 4 Hz frequency, (b) SMG920V#1 with a sinusoidal excitation of 25.6 mm peak-to-peak amplitude and 5 Hz frequency, (c) SMG920V#2 with a sinusoidal excitation of 18.2 mm peak-to-peak amplitude and 6 Hz frequency, and (d) SMG920V#2 with a sinusoidal excitation of 13.0 mm peak-to-peak amplitude and 7 Hz frequency.

Table 4.2: Experimental parameters and accuracy achieved by each phone represented by the standard deviation of the error (σ_e). Excitation in the form of sinusoidal shaking of different amplitudes and frequencies was applied to the shake table.

shaking frequency (Hz)	peak-to-peak amplitude (mm)	SMG900T σ_e (mm)	SMG920V#1 σ_e (mm)	SMG920V#2 σ_e (mm)
4	34.7	0.47	0.40	0.46
5	25.6	0.86	0.84	0.87
6	18.2	0.85	0.80	0.84
7	13.0	0.75	0.74	0.72

in [44]:

$$\begin{aligned}
 p_e = & (P(CP|IO) + P(CL|IO))P(IO) \\
 & + (P(IO|CP) + P(CL|CP))P(CP) \\
 & + (P(IO|CL) + P(CP|CL))P(CL),
 \end{aligned} \tag{4.7}$$

where $P(CP|IO)$ is the probability that the system classifies the building as CP , while its true classification is IO . $P(IO)$, $P(CP)$, and $P(CL)$ are the portion of buildings that have peak IDRs below 0.7%, between 0.7% and 5%, and above 5%, respectively. $P(IO)$, $P(CP)$, and $P(CL)$ are calculated using the classification limits in Table 1.2 and the typical peak inter-story drifts for several types of buildings under earthquake excitations of different intensities. As discussed in Appendix A, the peak inter-story drifts can be approximated as a normal distribution with a specific mean and variance for each hazard level, $\mathcal{N}(\mu_s, \sigma_s^2)$; the values of which are reported in Appendix A.

In practice, to evaluate the performance of a given SHM system, the following information is necessary:

1. the expected (typical) inter-story drifts for several types of buildings under earthquake excitations of different intensities (reported in Figure A.2).
2. the expected error in estimating the inter-story drift using the SHM system (reported in Table 4.2).
3. the classification boundaries that map inter-story drifts to the structural health state of the building (reported in Table 1.2).

Figure 4.9 presents the p_e of the SHM system in different scenarios. The p_e was calculated using Equation (4.7) for each earthquake intensity (i.e., for each distribution of inter-story drifts with a specific μ_s and σ_s ; $\mathcal{N}(\mu_s, \sigma_s^2)$). The p_e of the proposed SHM system is plotted as white-edged heat-scale grid in Figure 4.9. Additionally, p_e values for the hazard levels, corresponding to 2% probability of exceedance in 50 years, 10% probability of exceedance in 50 years, and 50% probability of exceedance in 50 years, are listed in Table 4.3 and highlighted in Figure 4.9. As expected, misclassification was highest when the IDRs were densely clustered around classification boundaries, such as the peak at $\mu_s = 2.8$ cm, which is equivalent to $\text{IDR} = 0.7\%$ (the boundary between IO and CP). The proposed multi-sensory SHM system achieved high performance ($p_e \leq 0.005$) for almost all hazard levels. The proposed system achieved a slightly lower performance ($p_e \approx 0.02$) when IDRs were highly clustered at the classification boundaries.

The performance of the proposed system was then compared with the performance of two other SHM systems: one that uses a network of seismic-grade accelerometers (KB12VD [63]) and one that uses a network of smartphones' internal accelerometers (MPU-6500 [62]). Figure 4.9 shows that the proposed system achieved a slightly lower (but comparable) performance than the system using seismic-grade accelerometers (black-edged gray grid in Figure 4.9); however, they both achieve the desired SHM accuracy reported in [33, 34] and [20]. A trade-off exists for accuracy with complexity and cost. For vulnerable buildings where extra

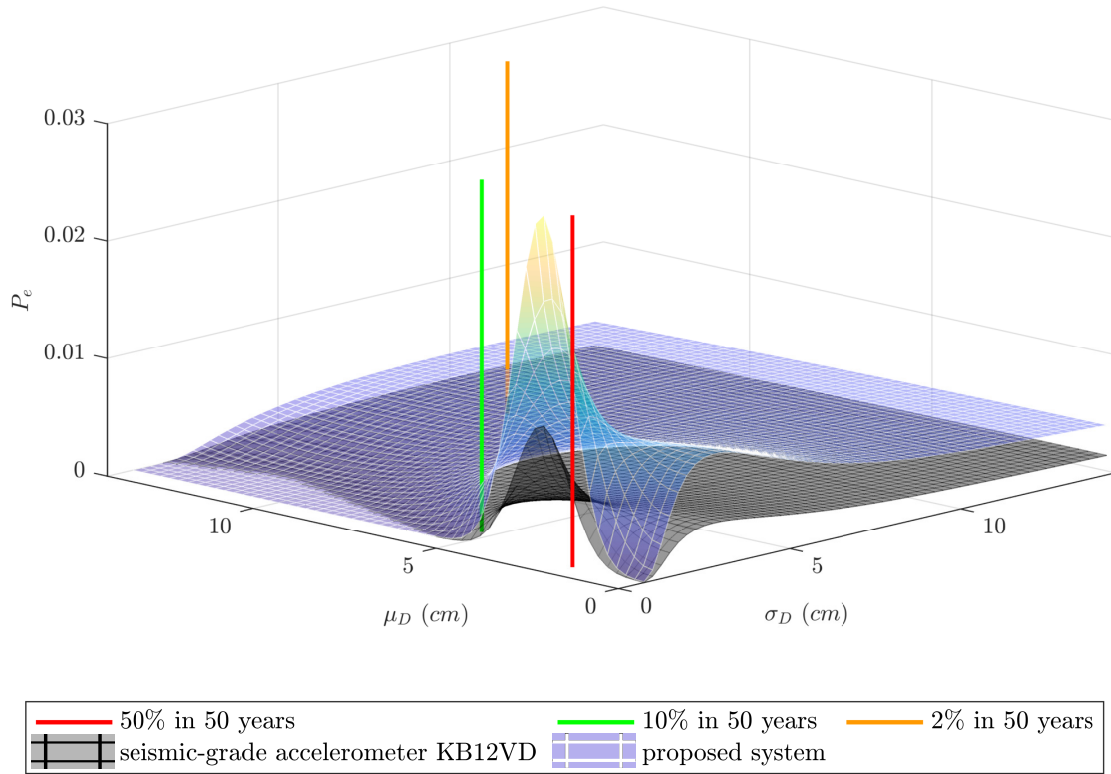


Figure 4.9: The performance of the proposed SHM system, plotted as the p_e for different distributions of inter-story drifts with a specific μ_s and σ_s (i.e., for different building types and under earthquake excitations of different intensities). The expected p_e values when an 8-story building is hit by an earthquake with hazard levels corresponding to a 2% probability of exceedance in 50 years, 10% in 50 years, and 50% in 50 years are highlighted in the plot. The performance of the system that uses seismic-grade accelerometers (KB12VD) is plotted for comparison.

accuracy is needed, the use of high-vitality seismic-tailored sensors, such as KB12VD, is recommended. Table 4.3 shows that the system that uses smartphones' internal accelerometers does not achieve the suggested SHM accuracy.

Table 4.3: Probability of structural damage classification error p_e using the proposed SHM system for different earthquake hazard levels; p_e values for other SHM systems for the same earthquake hazard levels are listed for comparison.

SHM system based on	p_e (50% in 50 years)	p_e (10% in 50 years)	p_e (2% in 50 years)
Seismic-grade accelerometer KB12VD [63]	0.0057	0.0018	0.0015
Proposed multi-sensory SHM	0.0146	0.0048	0.0038
Phone internal accelerometer MPU-6500 [62]	0.6706	0.2892	0.3279

4.5 Conclusions

A community-based multi-sensory SHM system was developed to allow for the large-scale monitoring of buildings after earthquakes. The system consists of a smartphone application and a cloud server. The app uses a smartphone’s internal accelerometer to detect earthquakes and trigger both a recording of the acceleration data and video footage. The acceleration data and the video footage are then fused in order to estimate the inter-story drift of the building in question, which is directly related to the structural safety of the building. This method avoids the need for an off-structure reference point, and is insensitive to weather conditions and visibility range. Damaged buildings are reported to emergency personnel as well as to the public in the form of a disaster map, with buildings tagged by their most likely health state. Validated by shake table experiments, the proposed SHM systems achieve sub-millimeter accuracy, far exceeding structural monitoring standards. The probability of

classification errors using the proposed SHM system is discussed and compared with that of other SHM systems. The analysis showed that the proposed system achieves comparable accuracy to seismic-grade accelerometers in the identification of structural damage.

Conclusion

A community-based multi-sensory SHM system was developed to allow for the large-scale monitoring of buildings after earthquakes. The system consists of a smartphone application and a cloud server. The app uses a smartphone's internal accelerometer to detect earthquakes and trigger both a recording of the acceleration data and video footage. The acceleration data and the video footage are then fused in order to estimate the inter-story drift of the building in question, which is directly related to the structural safety of the building. To the best of our knowledge, using smartphone cameras within a structure to monitor the response of floors during earthquakes is a novel technique. This method avoids the need for an off-structure reference point, and is insensitive to weather conditions and visibility range. Damaged buildings are reported to emergency personnel as well as to the public in the form of a disaster map, with buildings tagged by their most likely health state.

Validated by shake table experiments, the proposed SHM systems achieve sub-millimeter accuracy, far exceeding structural monitoring standards. The probability of classification errors using the proposed SHM system is discussed and compared with that of other SHM systems. The analysis showed that the proposed system achieves comparable accuracy to a system that used costly seismic-grade accelerometers in the identification of structural damage. While using high-fidelity SHM systems to monitor all buildings in earthquake-prone areas is optimal, achieving that goal is infeasible with respect to cost and deployment time. The proposed system is intended to be used in buildings that currently do not use

any form of SHM (in some cases, because they are awaiting instrumentation), which are the majority of buildings in the USA and around the world.

Bibliography

- [1] Piezotronics model 393c datasheet.
- [2] American Society of Civil Engineers. *Seismic rehabilitation of existing buildings*, volume 41, page 12. ASCE Publications, 2007.
- [3] Shannon Doocy, Amy Daniels, Catherine Packer, Anna Dick, and Thomas D Kirsch. The human impact of earthquakes: a historical review of events 1980-2009 and systematic literature review. *PLoS currents*, 5, 2013.
- [4] Kishor S Jaiswal, Mark D Petersen, Ken Rukstales, and William S Leith. Earthquake shaking hazard estimates and exposure changes in the conterminous united states. *Earthquake Spectra*, 31(S1):S201–S220, 2015.
- [5] ST Detweiler and AM Wein. The haywired earthquake scenario–engineering implications. Technical report, Tech. Rep., Reston, VA, 2018.
- [6] Meera Raghunandan, Abbie B Liel, and Nicolas Luco. Aftershock collapse vulnerability assessment of reinforced concrete frame structures. *Earthquake Engineering & Structural Dynamics*, 44(3):419–439, 2015.
- [7] Charles R Farrar and Keith Worden. An introduction to structural health monitoring. *Philosophical Transactions of the Royal Society A: Mathematical, Physical and Engineering Sciences*, 365(1851):303–315, 2007.
- [8] Andrew R Scott. Characterizing system health using modal analysis. *IEEE Transactions on Instrumentation and Measurement*, 58(2):297–302, 2008.
- [9] Filippo Ubertini, Simon Laflamme, Eleni Chatzi, Branko Glisic, and Filipe Magalhaes. Dense sensor networks for mesoscale shm: innovations in sensing technologies and signal processing. *Measurement Science and Technology*, 28(4):040103, 2017.
- [10] Alessandro Sabato, Christopher Niezrecki, and Giancarlo Fortino. Wireless mems-based accelerometer sensor boards for structural vibration monitoring: a review. *IEEE Sensors Journal*, 17(2):226–235, 2016.
- [11] OS Salawu. Detection of structural damage through changes in frequency: a review. *Engineering structures*, 19(9):718–723, 1997.

- [12] Devaka Jayawardana, Sergey Kharkovsky, Ranjith Liyanapathirana, and Xinqun Zhu. Measurement system with accelerometer integrated rfid tag for infrastructure health monitoring. *IEEE Transactions on instrumentation and measurement*, 65(5):1163–1171, 2015.
- [13] Devaka Jayawardana, Ranjith Liyanapathirana, and Xinqun Zhu. Rfid-based wireless multi-sensory system for simultaneous dynamic acceleration and strain measurements of civil infrastructure. *IEEE Sensors Journal*, 19(24):12389–12397, 2019.
- [14] Federica Zonzini, Michelangelo Maria Malatesta, Denis Bogomolov, Nicola Testoni, Alessandro Marzani, and Luca De Marchi. Vibration-based shm with up-scalable and low-cost sensor networks. *IEEE Transactions on Instrumentation and Measurement*, 2020.
- [15] Gennaro Magliulo, Vincenzo Pentangelo, Giuseppe Maddaloni, Vittorio Capozzi, Crescenzo Petrone, Pauline Lopez, Renato Talamonti, and Gaetano Manfredi. Shake table tests for seismic assessment of suspended continuous ceilings. *Bulletin of Earthquake Engineering*, 10(6):1819–1832, 2012.
- [16] Carlo Rainieri, Danilo Gargaro, and Giovanni Fabbrocino. Hardware and software solutions for seismic shm of hospitals. In *Seismic Structural Health Monitoring*, pages 279–300. Springer, 2019.
- [17] Derek A Skolnik and John W Wallace. Critical assessment of interstory drift measurements. *Journal of structural engineering*, 136(12):1574–1584, 2010.
- [18] Bekir Bulent Algan. *Drift and damage considerations in earthquake-resistant design of reinforced concrete buildings*. PhD thesis, University of Illinois at Urbana-Champaign, 1982.
- [19] Yousef Bozorgnia and Vitelmo V Bertero. Improved shaking and damage parameters for post-earthquake applications. In *Proceedings, SMIP01 seminar on utilization of strong-motion data, Los Angeles*, pages 1–22. Citeseer, 2001.
- [20] Alexander Charles Amies, Christopher G Pretty, Geoffrey W Rodgers, and J Geoffrey Chase. Experimental validation of a radar-based structural health monitoring system. *IEEE/ASME Transactions on Mechatronics*, 24(5):2064–2072, 2019.
- [21] Darragh Lydon, Myra Lydon, Jesús Martínez del Rincón, Susan E Taylor, Desmond Robinson, Eugene O’Brien, and F Necati Catbas. Development and field testing of a time-synchronized system for multi-point displacement calculation using low-cost wireless vision-based sensors. *IEEE Sensors Journal*, 18(23):9744–9754, 2018.
- [22] Niannian Wang, Kwang Ri, Hao Liu, and Xuefeng Zhao. Structural displacement monitoring using smartphone camera and digital image correlation. *IEEE Sensors Journal*, 18(11):4664–4672, 2018.
- [23] Dongming Feng, Maria Q Feng, Ekin Ozer, and Yoshio Fukuda. A vision-based sensor for noncontact structural displacement measurement. *Sensors*, 15(7):16557–16575, 2015.

- [24] SW Park, Hyo Seon Park, JH Kim, and Hojjat Adeli. 3d displacement measurement model for health monitoring of structures using a motion capture system. *Measurement*, 59:352–362, 2015.
- [25] Yang Zhang, Xuefeng Zhao, and Peng Liu. Multi-point displacement monitoring based on full convolutional neural network and smartphone. *IEEE Access*, 7:139628–139634, 2019.
- [26] Maria Pina Limongelli and Mehmet Çelebi. *Seismic Structural Health Monitoring: From Theory to Successful Applications*. Springer, 2019.
- [27] Jack Reilly, Shideh Dashti, Mari Ervasti, Jonathan D Bray, Steven D Glaser, and Alexandre M Bayen. Mobile phones as seismologic sensors: Automating data extraction for the ishake system. *IEEE Transactions on Automation Science and Engineering*, 10(2):242–251, 2013.
- [28] Qingkai Kong, Richard M Allen, Louis Schreier, and Young-Woo Kwon. Myshake: A smartphone seismic network for earthquake early warning and beyond. *Science advances*, 2(2):e1501055, 2016.
- [29] Qingkai Kong, Sarina Patel, Asaf Inbal, and Richard M Allen. Myshake: Detecting and characterizing earthquakes with a global smartphone seismic network. *arXiv preprint arXiv:1904.09755*, 2019.
- [30] Elizabeth Cochran, Jesse Lawrence, Carl Christensen, and Angela Chung. A novel strong-motion seismic network for community participation in earthquake monitoring. *IEEE Instrumentation & Measurement Magazine*, 12(6):8–15, 2009.
- [31] MD Kohler, R Guy, J Bunn, A Massari, R Clayton, T Heaton, KM Chandy, H Ebrahimian, and C Dorn. Community seismic network and localized earthquake situational awareness. 2018.
- [32] Community seismic network (csn).
- [33] Carlos M Ramirez, Dimitrios G Lignos, Eduardo Miranda, and Dimitrios Kolios. Fragility functions for pre-northridge welded steel moment-resisting beam-to-column connections. *Engineering structures*, 45:574–584, 2012.
- [34] Jack W Baker. Efficient analytical fragility function fitting using dynamic structural analysis. *Earthquake Spectra*, 31(1):579–599, 2015.
- [35] Getting raw accelerometer events — apple developer documentation.
- [36] Network time protocol website.
- [37] David L Mills. Internet time synchronization: the network time protocol. *IEEE Transactions on communications*, 39(10):1482–1493, 1991.

- [38] Simon Ostermann, Alexandria Iosup, Nezh Yigitbasi, Radu Prodan, Thomas Fahringer, and Dick Epema. A performance analysis of ec2 cloud computing services for scientific computing. In *International Conference on Cloud Computing*, pages 115–131. Springer, 2009.
- [39] Building Seismic Safety Council. Nehrps recommended seismic design criteria for new steel moment-frame buildings. *FEMA-273, Federal Emergency Management Agency, Washington, DC*, 2000.
- [40] Matthew Faulkner, Michael Olson, Rishi Chandy, Jonathan Krause, K Mani Chandy, and Andreas Krause. The next big one: Detecting earthquakes and other rare events from community-based sensors. In *Proceedings of the 10th ACM/IEEE International Conference on Information Processing in Sensor Networks*, pages 13–24. IEEE, 2011.
- [41] Shideh Dashti, Jonathan D Bray, Jack Reilly, Steven Glaser, Alexandre Bayen, and Ervasti Mari. Evaluating the reliability of phones as seismic monitoring instruments. *Earthquake Spectra*, 30(2):721–742, 2014.
- [42] Qingkai Kong, Young-Woo Kwony, Louis Schreierz, Steven Allen, Richard Allen, and Jennifer Strauss. Smartphone-based networks for earthquake detection. In *2015 15th International Conference on Innovations for Community Services (I4CS)*, pages 1–8. IEEE, 2015.
- [43] Asaf Inbal, Qingkai Kong, William Savran, and Richard M Allen. On the feasibility of using the dense myshake smartphone array for earthquake location. *Seismological Research Letters*, 90(3):1209–1218, 2019.
- [44] Ahmed Ibrahim, Ahmed Eltawil, Yunsu Na, and Sherif El-Tawil. Effect of sensor error on the assessment of seismic building damage. *IEEE Transactions on Instrumentation and Measurement*, 2019.
- [45] A. Ibrahim, A. Eltawil, Y. Na, and S. El-Tawil. Accuracy limits of embedded smart device accelerometer sensors. *IEEE Transactions on Instrumentation and Measurement*, 69(8):5488–5496, 2020.
- [46] Miroslav Trajković and Mark Hedley. Fast corner detection. *Image and vision computing*, 16(2):75–87, 1998.
- [47] Hiram Badillo-Almaraz, Andrew S Whittaker, and Andrei M Reinhorn. Seismic fragility of suspended ceiling systems. *Earthquake Spectra*, 23(1):21–40, 2007.
- [48] Carlo Tomasi and T Kanade Detection. Tracking of point features. Technical report, Tech. Rep. CMU-CS-91-132, Carnegie Mellon University, 1991.
- [49] Yunsu Na, Sherif El-Tawil, Ahmed Ibrahim, and Ahmed Eltawil. Stick-slip classification based on machine learning techniques for building damage assessment. *Journal of Earthquake Engineering*, pages 1–18, 2021.

- [50] Yunsu Na, Sherif El-Tawil, Ahmed Ibrahim, and Ahmed Eltawil. Automated assessment of building damage from seismic events using smartphones. *Journal of Structural Engineering*, 146(5):04020076, 2020.
- [51] Yunsu Na, Sherif El-Tawil, Ahmed Ibrahim, and Ahmed Eltawil. Identifying stick-slip characteristics of a smart device on a seismically excited surface using on-board sensors. *Journal of Earthquake Engineering*, pages 1–19, 2019.
- [52] YI Xiao, Wen-Xue Wang, Yoshihiro Takao, and Takashi Ishikawa. The effective friction coefficient of a laminate composite, and analysis of pin-loaded plates. *Journal of composite materials*, 34(1):69–87, 2000.
- [53] WM McKenzie and H Karpovich. The frictional behaviour of wood. *Wood science and technology*, 2(2):139–152, 1968.
- [54] Olga P Terleeva, Aleksandra I Slonova, Aleksey B Rogov, Allan Matthews, and Aleksey Yerokhin. Wear resistant coatings with a high friction coefficient produced by plasma electrolytic oxidation of al alloys in electrolytes with basalt mineral powder additions. *Materials*, 12(17):2738, 2019.
- [55] Farzad Naeim. Performance of extensively instrumented buildings during the january 17, 1994 northridge earthquake. *An Interactive Information System, Report No. 97*, 7530, 1997.
- [56] HM Antia. *Numerical methods for scientists and engineers*, volume 2. Springer, 2012.
- [57] N Fukuwa, R Nishizaka, S Yagi, K Tanaka, and Y Tamura. Field measurement of damping and natural frequency of an actual steel-framed building over a wide range of amplitudes. *Journal of wind engineering and industrial aerodynamics*, 59(2-3):325–347, 1996.
- [58] Yanchun Ni, Xilin Lu, and Wensheng Lu. Operational modal analysis of a high-rise multi-function building with dampers by a bayesian approach. *Mechanical Systems and Signal Processing*, 86:286–307, 2017.
- [59] Smg900t datasheet.
- [60] Smg920v datasheet.
- [61] Mpu-6050 six-axis (gyro + accelerometer) mems motiontracking devices.
- [62] Mpu-6500 six-axis (gyro + accelerometer) mems motiontracking devices.
- [63] Kb12vd accelerometer datasheet.
- [64] Charles Kircher, Gregory Deierlein, John Hooper, Helmut Krawinkler, Steve Mahin, Benson Shing, and John Wallace. Evaluation of the fema p-695 methodology for quantification of building seismic performance factors. Technical report, 2010.

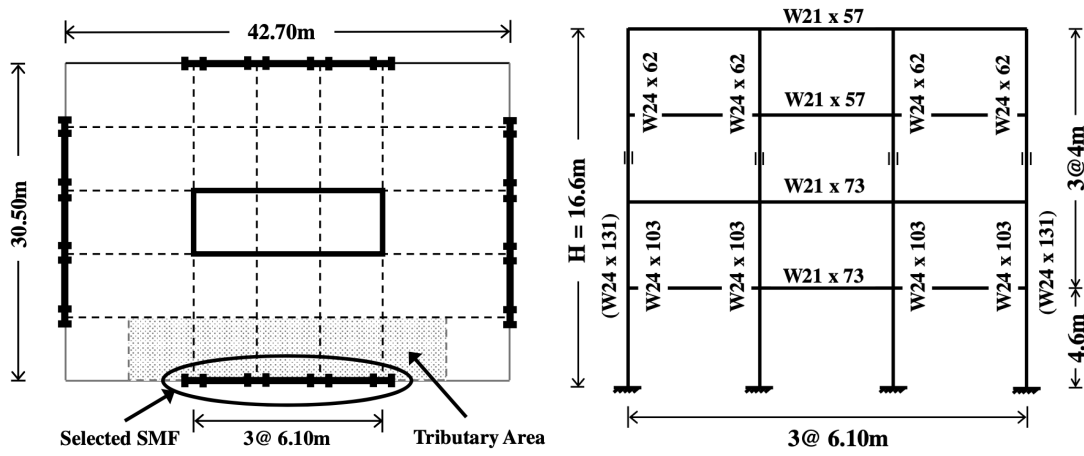
- [65] Dominic Kelly. Seismic site classification for structural engineers. *Structure*, 21:21–24, 2006.
- [66] Altair engineering, hypermesh.
- [67] Livermore software technology corporation, ls-dyna.
- [68] Tung-Yu Wu, Sherif El-Tawil, and Jason McCormick. Seismic collapse response of steel moment frames with deep columns. *Journal of Structural Engineering*, 144(9):04018145, 2018.
- [69] Applied Technology Council and United States. Federal Emergency Management Agency. *Quantification of Building Seismic Performance Factors*. U.S. Department of Homeland Security, FEMA, 2009.

Appendix A

Inter-Story Drift Distribution

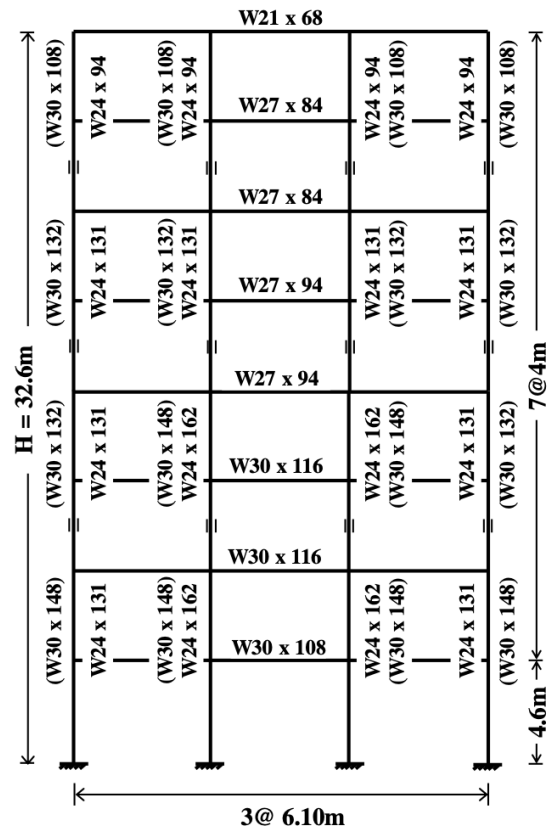
Building responses under earthquake excitation were simulated to model the inter-story drift distributions. Four- and eight-story steel-frame buildings designed by NIST [64] were considered in the simulation; the buildings' plans are presented in Figure A.1. The lateral load-resisting system used in the building consisted of three-bay perimeter steel special-moment frames (SMFs) with reduced beam sections on each side of the building. Site class D, the most common site class throughout the United States [65], is a mixture of dense clay, silt, and sand, and was used as the type of soil in the simulated construction site. Finite element models of the SMFs were created using HyperMesh [66] and analyzed using the commercial code LS-DYNA [67]. The steel used in the building was ASTM-A992; its engineering stress–strain properties were converted into true stress–strain data, then assigned to the finite elements. A mass weighted damping of 2.5% was assumed at the first mode period of the SMFs. Additional modeling details are provided in [68].

The distributions of peak relative displacement were computed for three seismic hazard levels: 2% probability of exceedance in 50 years, 10% in 50 years, and 50% in 50 years. Eleven seismic records were selected from the far-field ground motion record set in FEMA [69] and



(a)

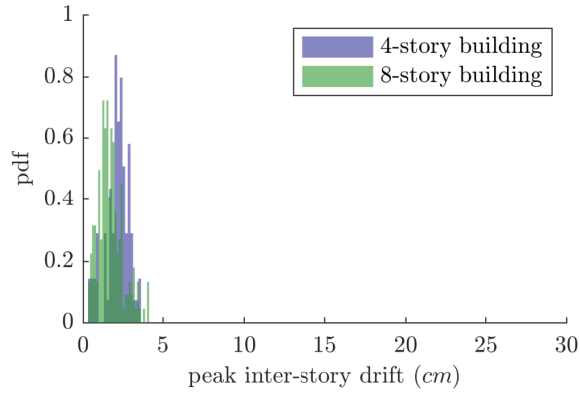
(b)



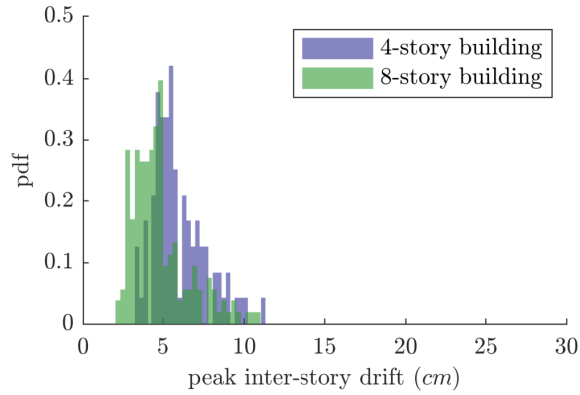
(c)

Figure A.1: (a) Plan configuration, (b) elevation view of a 4-story prototype special-moment frame (SMF), and (c) elevation view of an 8-story prototype SMF.

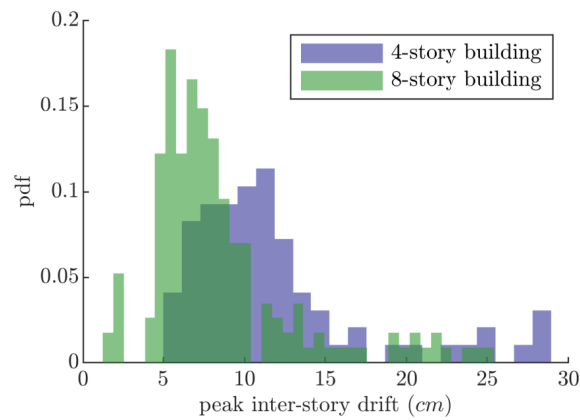
scaled to the three specified hazard levels, resulting in 33 records. Each building was then subjected to the scaled seismic records for each hazard level and the peak relative displacement was computed. The histogram of peak relative displacement is shown in Figure A.2. The distribution can be approximated as Gaussian with a mean of μ_s and a variance of σ_s^2 , $\mathbf{s}_t \sim \mathcal{N}(\mu_s, \sigma_s^2)$, depending on the hazard level, with slight variations depending on the building type.



(a) $\mu_s \approx 1.92 \text{ cm}$, $\sigma_s \approx 0.72 \text{ cm}$



(b) $\mu_s \approx 5.2 \text{ cm}$, $\sigma_s \approx 1.68 \text{ cm}$



(c) $\mu_s \approx 12 \text{ cm}$, $\sigma_s \approx 9.6 \text{ cm}$

Figure A.2: Histogram of peak relative displacement of 4- and 8-story moment frame steel buildings resulting from an earthquake intensity that corresponds to hazard levels of (a) a 50% probability of exceedance in 50 years, (b) 10% in 50 years, and (c) 2% in 50 years.